Chemical Geology 332–333 (2012) 45–64

Contents lists available at SciVerse ScienceDirect

Chemical Geology

journal homepage: www.elsevier.com/locate/chemgeo

Impact of diagenesis and low grade metamorphosis on isotope (δ^{26}Mg, δ^{13}C, δ^{18}O and ^{87}Sr/^{86}Sr) and elemental (Ca, Mg, Mn, Fe and Sr) signatures of Triassic sabkha dolomites

A. Geske *, J. Zorlu, D.K. Richter, D. Buhl, A. Niedermayr, A. Immenhauser

Ruhr-University Bochum, Institute for Geology, Mineralogy and Geophysics, Universitätsstraße 150, D-44801 Bochum, Germany

ARTICLE INFO

Article history:
Received 4 June 2012
Received in revised form 3 September 2012
Accepted 6 September 2012
Available online 14 September 2012

Editor: U. Brand

Keywords:
Dolomite
Geochemistry
Magnesium isotopes
Diagenesis

ABSTRACT

Dolomite is a common rock forming mineral in the geological record but its value as archive of ancient seawater δ^{26}Mg signatures and their variations in time is at present underexplored. Unknown factors include the sensitivity of δ^{26}Mg ratio to processes in the diagenetic and low grade metamorphic domain. This paper documents and discusses the first detailed δ^{26}Mg data set from early diagenetic and burial dolomites. Samples come from the Upper Triassic Hauptdolomit (Dolomia Principale; The Dolomites, Italy) and include coeval dolomicrites that underwent differential burial diagenesis and low grade metamorphosis in a temperature range between about 100 and more than 350 °C. Magnesium isotope data are complemented by dolomite δ^{13}C, δ^{18}O and ^{87}Sr/^{86}Sr isotope ratios as well as Ca, Mg, Mn, Fe and Sr elemental abundances and data on the dolomite crystal structure. As indicated by dolomicrite ^{87}Sr/^{86}Sr ratios and petrographic evidence, sabkha calcian D1 dolomites precipitated from evaporated seawater and stabilized at an early marine pore water diagenetic stage to D2 dolomites analysed here. With increasing burial temperature, dolomite δ^{26}Mg ratio scatter in the data set decreases with increasing Mg/Ca ratio and degree of order. Specifically, δ^{26}Mg ratio variability is reduced from $\pm$0.36‰ 2σ at burial temperatures beneath 100 °C to about $\pm$0.14‰ 2σ at temperatures in excess of 350 °C, respectively, with mean δ^{26}Mg values ranging constantly near −1.9‰. This suggests that, at least for the rock buffered system investigated here, dolomicrite δ^{26}Mg proxy data are conservative and preserve near pristine values even at elevated burial temperatures. At present, the main element of uncertainty is the Mg-isotope fractionation factor between (evaporated) seawater and dolomite. A possible solution to this problem includes the compilation of data from modern sabkha environments including pore water and calcian dolomite δ^{26}Mg isotope signatures.

1. Introduction

Dolomite is a common sedimentary rock-forming mineral in the geologic record but is absent in most Holocene and modern marine sediments. This discrepancy is described as “dolomite problem” and has triggered a lively discussion amongst carbonate sedimentologists and geochemists for more than 150 years (De Dolomieu, 1791; Haidinger, 1845; Nadson, 1928; Pisciotto and Mahoney, 1981; Purser et al., 1994; Vasconcelos et al., 1995; Deelman, 2011). Furthermore, the precipitation kinetics (e.g., Berástegui et al., 1998) of dolomite is still under debate. Burns et al. (2000) suggested that the distribution bias of marine dolomite through the Phanerozoic reflects a complex combination of changes in sea floor spreading rates, changing ocean pCO_2 levels, seawater Mg/Ca ratio and sulphate concentration as well as the activity of anaerobic microbes.

Magnesium is the key element of dolomite and an important element in the carbonate cycle (Warren, 2000). Published data of dolomite Mg isotope ratios, however, are at best scarce and a systematic analysis of the impact of diagenesis and low grade metamorphosis on dolomite δ^{26}Mg is at present lacking. To the knowledge of the authors, previous work that is of direct relevance here is limited to a conference abstract dealing with bacterially induced dolomite precipitation (Carder et al., 2005) and studies with focus on the Mg cycle (De Villiers et al., 2005; Tipper et al., 2006, 2008a, 2008b; Brenot et al., 2008; Jacobson et al., 2010; Pokrovsky et al., 2011). In addition, Galy et al. (2002) published δ^{26}Mg values of a dolostone host rock in a speleothem based study and Chang et al. (2003), Young and Galy (2004), Tipper et al. (2008a, 2008b) and Wombacher et al. (2009) investigated Mg purification techniques and δ^{26}Mg analysis using MC-ICP-MS in experimental studies. Rustad et al. (2010) and Schauble (2011) published data of theoretically calculated equilibrium Mg isotope fractionation factors of oxide, silicate and carbonate minerals.

The main source of Mg for dolomite precipitation is seawater. Consequently, the Mg concentration and the δ^{26}Mg isotopic composition of seawater are of particular interest. Modern ocean water Mg concentration and the δ^{26}Mg isotope signature is 53 mmol/l and −0.82‰, respectively (Young and Galy, 2004; Hippler et al., 2009; Higgins and Schrag, 2010; Ling et al., 2011). Previous research indicates a strong depletion of microbial dolomite δ^{26}Mg by up to 2–3‰ relative to the fluid from which they precipitated (Carder et al., 2005). In contrast to organic

* Corresponding author. Tel.: +49 234 3225457.
E-mail address: Anna.Geske@rub.de (A. Geske).

0009-2541/$ – see front matter © 2012 Elsevier B.V. All rights reserved.
http://dx.doi.org/10.1016/j.chemgeo.2012.09.014

precipitates, inorganic carbonates appear to show a small range of fractionation. Numerous studies deal with magnesium isotope fractionation associated with the precipitation of inorganic carbonates. Theoretical studies (Rustad et al., 2010; Schauble, 2011) and field observations (Galy et al., 2002; Higgins and Schrag, 2010; Immenhauser et al., 2010) disagree in some aspects and at present, it is not entirely clear if the solid or the fluid phase is enriched in light magnesium isotopes during carbonate precipitation. Furthermore, it is not sufficiently well understood whether dolomite and calcite have similar $\delta^{26}Mg_{carb-sol}$ fractionation or not and to which degree non-equilibrium isotope effects contribute to low or high $^{26}Mg/^{24}Mg$.

This study aims at improving the data base of dolomite Mg isotope signatures. The long-term objective is to establish potentially characteristic $\delta^{26}Mg$ signatures of dolomites representing different dolomitization models. In a first step, however, the sensitivity of the dolomite $\delta^{26}Mg$ isotope system to diagenesis (<200 °C) and low grade metamorphosis (>200 °C) must be tested and tipping points along diagenetic pathways need to be established. This is significant because it is widely believed that dolomites recrystallize during eo- and meso-diagenesis and thereby reset their original geochemical, crystallographic and textural properties (Malone et al., 1996). Understanding the influence of increasing diagenetic alteration on dolomite $\delta^{26}Mg$ is essential for the interpretation of dolomite-based seawater $\delta^{26}Mg$ time series data sets and the assessment of $\delta^{26}Mg$ isotope data in general. For this purpose, we took advantage of the extensive outcrops of the well-studied Carnian–Norian (Triassic) Hauptdolomit (Dolomia Principale) in the alpine realm of Austria and Northern Italy (Zorlu et al., 2007) precipitated as penecontemporaneous dolomite in a sabkha environment. Depending on the locality, coeval stratigraphic units of the Hauptdolomit that experienced differential burial depths and burial fluid temperatures, detailed in the literature, were sampled (Kralik et al., 1987; Kürmann and Richter, 1989; Henrichs and Richter, 1993; Gawlick and Königshof, 1993; Kürmann, 1993; Gawlick et al., 1994; Gawlick, 1996).

Here, we report on the impact of diagenetic and metamorphic fluids on early diagenetic sabkha type dolomite $\delta^{26}Mg$ ratios in a temperature range between about 100 and >350 °C at a low pressure regime. Whilst the main focus is on the Mg isotope system and the crystal structure of the dolomites investigated, we also report and discuss supporting data on carbon, oxygen and strontium isotope ratios as well as main and trace elemental abundances.

2. Regional geo-tectonic, stratigraphic and sedimentologic framework

In this study, samples from the Norian (Upper Triassic) Hauptdolomit in the Austroalpine and Southern Alps of Austria and Italy (Tollmann, 1977) were analysed. The Norian Hauptdolomit is a regionally very extensive, stratigraphically thick (2000–2500 m) sedimentary succession of mainly dolostones, subordinate intervals of limestone and in places clayey–bituminous carbonates and marls (Fruth and Scherreiks, 1984).

Due to changing Norian sea level and the wide regional distribution of this unit, the Hauptdolomit platform recorded several stages of deepening and shallowing along the northern passive continental margin of the Adriatic plate (Gwinner, 1978; Fruth and Scherreiks, 1984; Ziegler, 1988; Gawlick and Frisch, 2003). The Triassic world differed, due to its plate tectonic framework, considerably from the modern one (Scotese, 2000; Gawlick and Frisch, 2003; Preto et al., 2010). Specifically, the Hauptdolomit facies formed in spatially very extensive, highly arid shallow marine settings at the western extension of the Tethys (Müller-Jungbluth, 1970; Bechstädt and Mostler, 1976; Brandner and Resch, 1981; Dercourt et al., 1993; Budd, 1997). In addition, a limited part of the Hauptdolomit dolostones accumulated in an intertidal to subtidal environment (Müller-Jungbluth, 1970).

Petrographic and sedimentological evidence for the deposition of the Hauptdolomite facies in a sabkha environment (Frisia, 1994; Iannace and Frisia, 1994) includes silicified sulphate nodules within micritic dolomite layers, thin gypsum layers observed in outcrops and an anhydrite phase found in many thin sections (Zorlu, 2006; Zorlu et al., 2007; see Fig. 1 for details). The silicified sulphate nodules are equivalents of the "chicken wire" structures found in recent sabkha dolomites of for example the gulf region near Abu Dhabi (Purser, 1973; McKenzie, 1981) and of the Shark Bay in Australia (Warren, 1991).

In analogy to modern case settings, two factors arguably drove dolomite precipitation in the Hauptdolomit sabkha environment. These are i) evaporative pumping and ii) surface flooding (McKenzie et al., 1980; McKenzie, 1981; McKenzie, 1990; see discussion in Morrow, 1982). In modern sabkha environments, saline floodwater brines sink downward and then flow seaward by seepage reflux. Evaporation of the mixed groundwater/seawater pore fluids with salinities of 200–400‰ results in the precipitation of anhydrite, gypsum and halite. Precipitation of these minerals removes sulphur and calcium from the 20–40 °C warm pore solution. The initial Mg/Ca ratio of the solution controls the rate of dolomitization and the dolomite stoichiometry (Kaczmarek and Sibley, 2011). The high magnesium concentration of these brines leads to early diagenetically dolomite precipitation within the supratidal zone. Typically, dolomites accumulate within calcareous muds less than a metre beneath the sabkha surface (Warren, 2000; Warthmann et al., 2000; Sánchez-Román et al., 2008, 2009; Lokier and Steuber, 2009; Bontognali et al., 2010). Following previous work, we here apply the sabkha dolomitization model (Morrow, 1982; Land, 1985) to the dolomicrites investigated.

The Hauptdolomit presently crops out in the Northern limestone Alps, the Western and Central Eastern Alps and the Southern Alps (Kübler and Müller, 1962; Geyssant, 1973; Dössegger and Müller, 1976; Gwinner, 1978; Dössegger et al., 1982; Kürmann, 1993; Bossellini, 1998) (Fig. 2). A geological sketch map indicating all sampling localities is shown in Fig. 3. The differential thermal gradients of sampling sites in the Northern Calcareous Alps and the Dolomites are the results of burial related to pre- or syn-tectonic alpine deformation. All sampling locations (Fig. 3) experienced Late Cretaceous metamorphism (K/Ar whole rock ages of 90–85 Ma; Ferreiro-Mählmann, 1994; Handy and Oberhänsli, 2004; Schuster et al., 2004). In addition to Cretaceous metamorphism, the sampling locations underwent a pre-tectonic truncation in the Paleogene that is associated with hydrothermal activity (29–43 Ma; Handy and Oberhänsli, 2004). Samples from the central Alps (sampling locations 4 and 5) were subject to a tectonic event described as the "Schneeberg Crystallisation" (Tollmann, 1977; Zeeh, 1998, 2000; Handy and Oberhänsli, 2004; Schuster et al., 2004). Thermal gradients of the different sampling locations are based on illite crystallinity, vitrinite reflectance, conodont colour alteration indices (CCAI) and calcite–dolomite-geothermometry (Buntebarth and Stegena, 1986; Anovitz and Essene, 1987). All of these methods provide approximate temperature ranges shown here in degree Celsius burial temperature.

3. Methods and materials

3.1. Sampling strategy

The selection of the Hauptdolomit as a target interval was motivated by (i) its widespread, homogenous mechanism of early diagenetic Sabkha dolomitization combined with (ii) well studied, regionally differential subsidence and thermal histories of sampling localities. Hand specimens were collected from five different sites in the alpine realm of Austria and northern Italy. Sampling sites were selected based on their well reconstructed thermal (burial) history ranging from 100 and about 350 °C as obtained from previous work.

From lowest to highest burial temperatures, the sampling sites include the Osterhorn block area (region 1; Northern Calcareous Alps; Kralik et al., 1987; Gawlick and Königshof, 1993; Gawlick et al., 1994; Gawlick, 1996) and the Sella and Mendel Pass region (sampling location 2; dolomites; Buggisch, 1978; Henrichs and Richter, 1993; Zattin et al., 2006). For sampling locations 1 and 2, burial temperatures of about

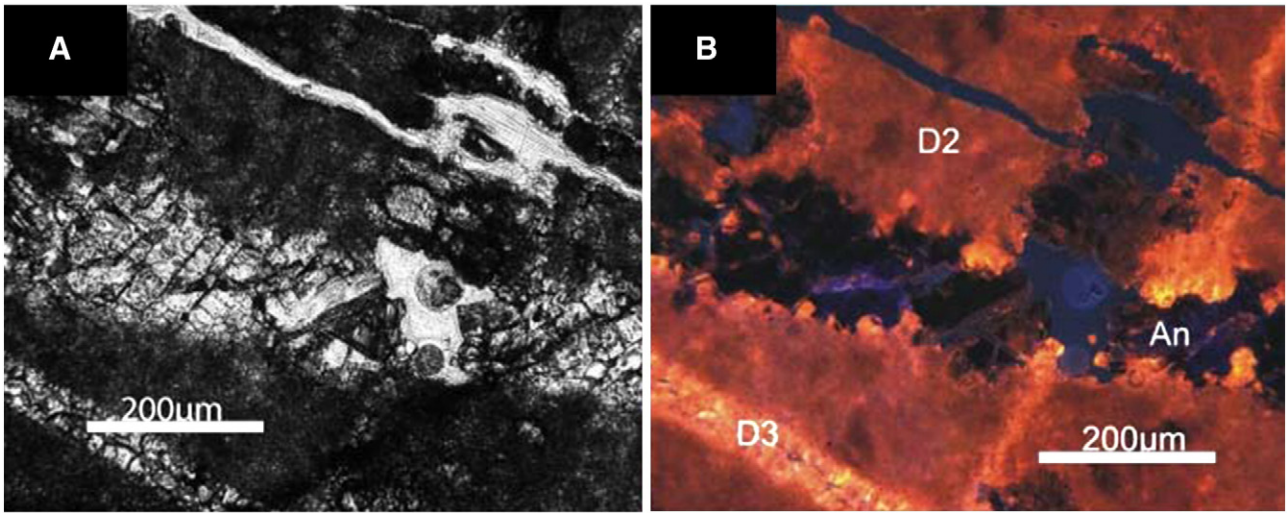

Fig. 1. A) Photomicrographs of Hauptdolomit phases D2 and D3. Evidence for the deposition of Hauptdolomit in a sabkha environment is provided by an anhydrite phase within petrogenetic dolomicrite D2 (scale = 200 µm). B) Same as A) but under cathodoluminescence (modified after Zorlu, 2006).

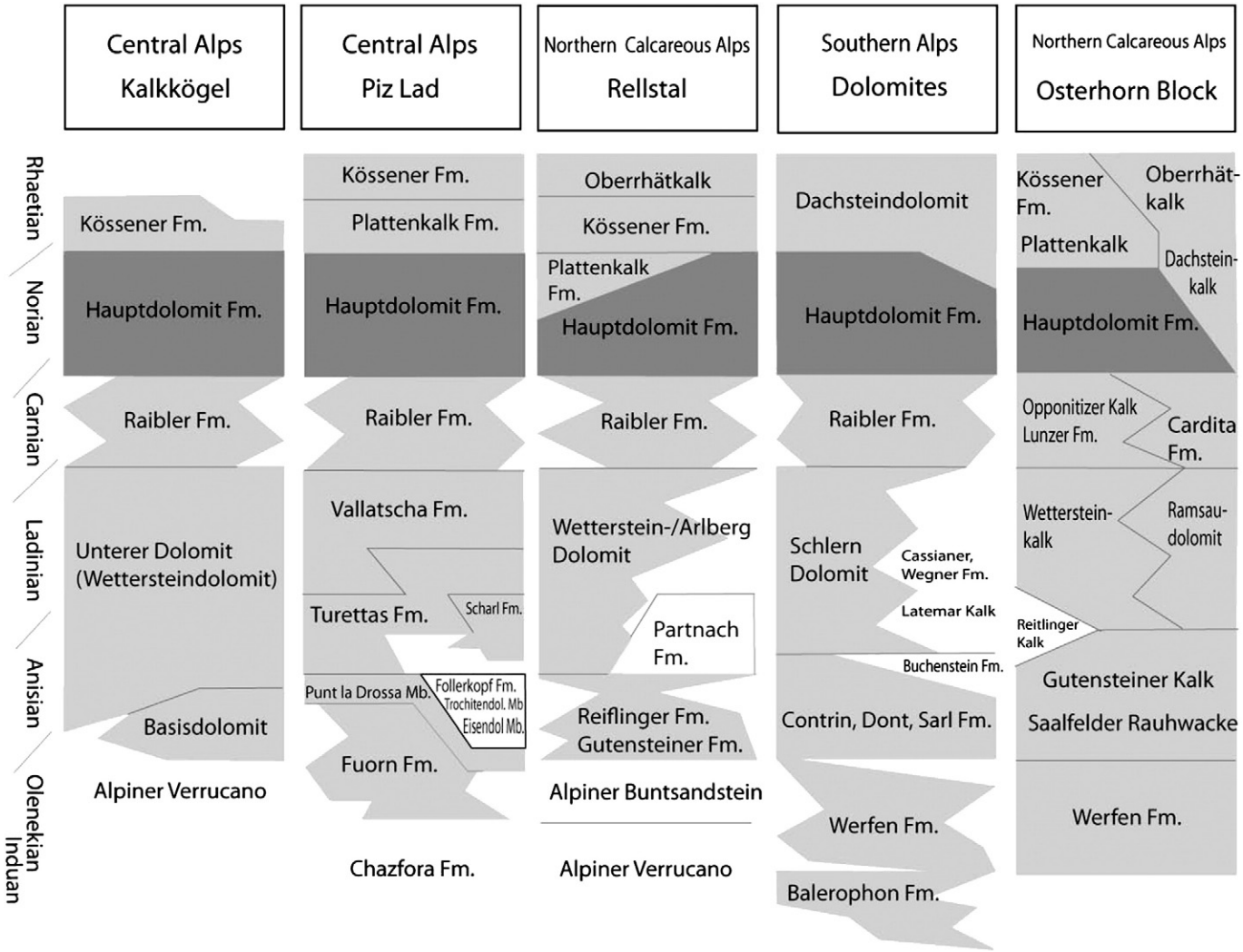

Fig. 2. Stratigraphic charts of the Northern Calcareous Alps (West; Rätikon and North, Osterhorn Block); the Unterengadiner Dolomites (Central Alps, Piz Lad); the Permomesozoic (Kalkkögel Block) and the Dolomites (Southern Alps; modified after Kübler and Müller, 1962; Geyssant, 1973; Dössegger and Müller, 1976; Gwinner, 1978; Dössegger et al., 1982; Kürmann, 1993; Bossellini, 1998).

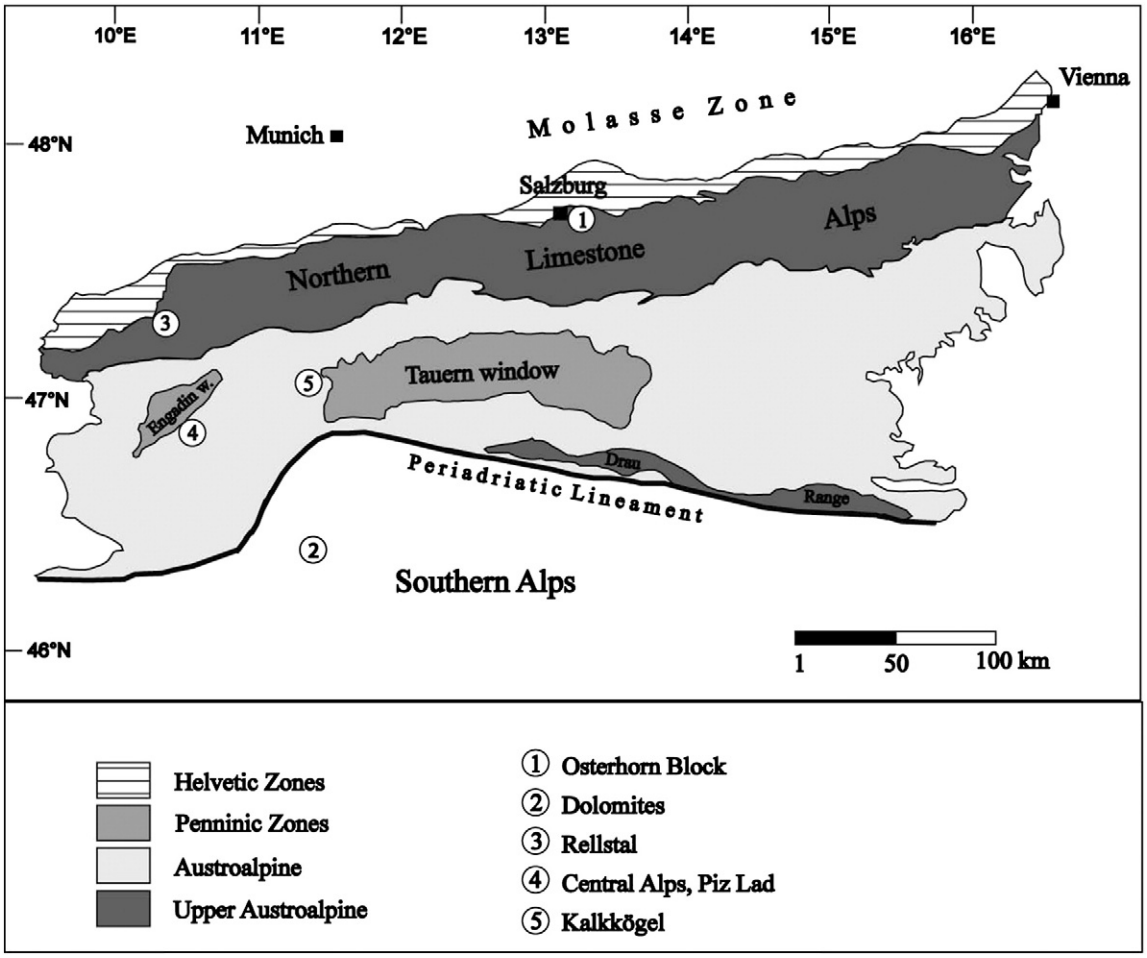

Fig. 3. Geological sketch map with locations of the five sampling sites of Triassic D2 dolomicrites and D4 saddle dolomites in the Eastern and Southern Alps (redrawn after Zorlu, 2006).

100 °C or less were reconstructed. Sampling location 3, the Rellstal valley (Northern Calcareous Alps; Kralik et al., 1987; Kürmann and Richter, 1989; Henrichs and Richter, 1993; Kürmann, 1993; Ferreiro-Mählmann, 1994) recorded burial temperatures in the order of 200 °C. Sampling location 4, the Piz Lad (Central Alps; Kürmann and Richter, 1989; Henrichs and Richter, 1993; Zorlu et al., 2007) represent maximum burial temperatures of around 300 °C. Sampling location 5, the Kalkögel area (Central Alps; Dietrich, 1980; Dietrich, 1983; Frank et al., 1987; Kürmann and Richter, 1989; Schmid and Haas, 1989; Henrichs and Richter, 1993; Donofrio, 2008) reached burial temperatures of approximately 350 °C. Refer to Figs. 2 and 3 for stratigraphic and regional information and the metamorphic map of the Alps (Oberhänsli et al., 2004) for mean burial temperatures.

3.2. Facies and dolomite phases

Based on field observations, Hauptdolomit samples investigated were subdivided into the following three basic facies types, whilst thin sections revealed a more diverse range of facies types: (i) mud- and wackestones, which are here referred to as type I facies. In hand specimen, type I dolostones appear macroscopically greyish to brownish and in the field carbonates are organized in beds ranging between 10 and 100 cm in thickness. This dolomite facies is often laminated, rich in bird's-eye structures, with laminae presumably formed by cyanobacteria mats (Zorlu et al., 2007). In thin sections, this facies contains well preserved bioclasts such as (dasycladacean/chlorophycean) algae and foraminifera, fine bivalve shell material and pelletal structures defined as "structure grumeleuse" according to Cayeux (1935). The depositional environment lies within the restricted Norian sabkha (supratidal) setting (Müller-Jungbluth, 1970).

Facies type II differs from type I by its substantial increased content and diversity of skeletal grains, forming dolomite pack- to grainstones (Müller-Jungbluth, 1970). Judging from the facies composition, the depositional environment ranges from the inter- to subtidal setting and points to a less restricted marine environment relative to type I. In outcrops, type I and II facies alternates stratigraphically. Sampling material used in this study is from facies types I and II. A third facies type (III), deposited in the subtidal domain, is found locally and includes bitumen-rich Ca-rich dolostone–shale alternations (Müller-Jungbluth, 1970). This facies type was not included into this study.

We here apply the subdivision of different dolomite phases as suggested in Zorlu et al. (2007). Given that the later reference is in German language, we here provide relevant details of the different phases in a condensed manner (Table 1). These authors propose four dolomite types (D1–D4) as based on detailed cathode luminescence investigations. Type D1 is defined as a weakly ordered, non-stoichiometric, dislocation-ridden proto-dolomite (sensu McKenzie, 1981; Mazullo et al., 1987; Frisia, 1994; Chafetz and Rush, 1994), which was subsequently replaced by calcian dolomite type D2 during a very early diagenetic stage (Zorlu et al., 2007). Type D2 is composed of crypto- to microcrystalline (1–4 μm) anhedral to subhedral, weak to intensely pigmented dolomicrite and a first generation of dolomite cement (5–15 μm;

Table 1
Classification of Hauptdolomit phases (after Zorlu, 2006 and Zorlu et al., 2007).

Label	Crystal size	Morphology	CL colours	Dolomite type	Inclusions
D2	1–4 μm (s.l.1) 5–15 μm (s.l.5)	Anhedral nonplanar	Brown-orange to pale-red	Dolomicrite	None
D3	>20–50 μm in fissures 50–300 μm (in pore space (saddle dolomite)	Sub-euhedral planar	Scarlet red	Coarser grained dolomicrite and saddle dolomite	Very abundant
D4	200–500 μm	Sub-euhedral/idiomorph	Red violet to wine red	Saddle dolomite	Abundant

s.l. = sampling location.

Fig. 4A–D), due to local accretive crystallisation. The later phase shows brownish- to yellowish-red and pale-red cathodoluminescence colours and fills fractures and pores. Dolomite type D3 (>20 μm) is characterized by scarlet luminescence colours and fills the secondary network of fissures. In pore space, this type of dolomite appears as rhombic, zoned, sub-euhedral crystals (50–300 μm) and as saddle dolomite. Type D4 dolomite cement is intensely pigmented, sub-euhedral and displays a red-violet to wine-red luminescence colour (Fig. 4E and F). This hydrothermal saddle dolomite phase (Zorlu et al., 2007) occludes the youngest network of fissures and pores. It is a non-planar to xenotopic dolomite (Gregg and Sibley, 1984; Sibley and Gregg, 1987) phase that consists of anhedral crystals of 200 to 500 μm in diameter. At the fringes of pores, this cement type is mainly found as a nonplanar dolomite mosaic whilst saddle dolomite dominates the centre of pores. According to Zorlu et al. (2007) D2 dolomites accumulated during the Triassic eogenetic stage, whilst D3 and D4 either formed meso- and telogenetically during the Late Cretaceous (D3) and the Paleogene to early Neogene (D4). In the context of this study, the earliest preserved diagenetic dolomite phase D2 (dolomicrite; Fig. 4A–D) and the latest diagenetic dolomite phase D4 (saddle dolomite; Fig. 4E and F; Table 1) were analysed.

3.3. Instrumentation and data reporting

3.3.1. Crystallographical methods

In order to characterize the crystal lattice of dolomites (stoichiometry and degree of order) and to define the purity of individual samples, all specimens selected for further geochemical analysis were investigated with the Phillips X'Pert MPD Theta-Theta X-Ray Diffractometer at the Ruhr-University Bochum, Germany. The X-ray source is a long-fine-focus, ceramic X-ray tube with a Cu anode producing Cu Kα wavelength of 1.5405 Å. The measurement conditions include high voltage of 45 kV, a current of 40 mA, an angular range from 20 to 40, a step size of 0.025°2θ and a counting time of 11 s. A graphite secondary monochromator was used to minimize the background noise. The main dolomite peak $d_{(104)}$ (30.96°2θ≙2.886 Å for an ideal stoichiometric dolomite) was corrected against the internal standard material quartz with a main peak $d_{(101)}$ at 26.64°2θ≙3.343 Å to define the Mg/Ca-ratio of the crystal lattice. The $CaCO_3$ content in mol% was calculated using the equation of Lumsden (1979):

$$N_{CaCO_3} = Md + B$$

where N represents the $CaCO_3$ content in mol%, M is 333,33, B is −911.99 and d is the main diffraction peak (104) in Ångström.

The degree of order (R) of each dolomite was calculated with the following equation:

$$R = Id_{(015)}/Id_{(110)}$$

whereby (I) is the intensity of the peaks (015) (superstructure peak) and (110) in counts per second (cps); Füchtbauer and Goldschmidt, 1965; Füchtbauer and Richter, 1988; Hardy and Tucker, 1988.

In order to select dolomite type D2 and D4 samples for further geochemical analysis, cathodoluminescence imaging was performed using a hot stage HC1-LM at the Ruhr-University Bochum (Neuser et al., 1996). Twenty-four thin sections sputtered with gold were analysed under hot stage cathodoluminescence. The instrument is linked to a Kappa DX 30C video camera system for recording digital images and with an EG&G triple grating spectrograph connected to a liquid-N_2 cooled CCD-detector. The acceleration voltage of the electron beam is 14 kV, and a beam current density between 5 and 10 μA/mm^2 is used for measurement. The vacuum of the pump is 5.0×10^{-4} mbar and the beam current is between 0.1 and 0.2 mA. Integration times for luminescence-spectra were commonly between 10 and 60 s. For more details refer to Richter et al. (2003).

3.3.2. Geochemical methods

Thirty-two dolomicrite (D2) samples were extracted from hand specimen for δ^{26}Mg analysis using a hand held drill in order to collect sample powder from 2 mm^3 drill pits. In addition, four hydrothermal saddle dolomite (D4) samples were drilled and analysed in order to establish the geochemical signature of the late burial (mesogenetic) dolomite phases. The required sample powder quantity for magnesium isotope analysis was determined using an inductively coupled plasma optical emission spectrometer (ICP-OES, Thermo Fisher Scientific iCAP 6500 DUO). Based on the detected magnesium content of the sample powder, approximately 0.5 mg of powder was weighted in. The samples were dissolved in 1 ml 6 M HCl (supra pure) and subsequently evaporated on a hot plate at >100 °C to dryness. In order to destroy organic compounds and minimize potential interferences related to complexation of cations, the samples were treated with 1 ml H_2O_2–HNO_3 1:1 mixture. The samples were evaporated on a hot plate at 60 °C and then were re-dissolved in 1 ml 1.25 N HCl. The Mg fraction was recovered using BioRad ion exchange resin AG50 W-X12 (200–400mesh) and quartz glass columns. Typically 50 μg of Mg passed through the ion exchange columns. The column eluation pattern was determined for each column using an IAPSO seawater test solution (diluted 1:1). The Mg yield exceeds 95%.

A 500 ppb Mg-solution in 3.5% HNO_3 was measured on a Thermo Fisher Scientific Neptune MC-ICP-MS. The difference between the Mg concentration of the standard and sample was kept within a 15% limit, which proved minimizing potential isobaric interferences from matrices (Galy et al., 2001). A positive effect on signal stability and reduction of matrix interferences was achieved by combining two desolvating systems an ApexIR (ESI) and an Aridus (Cetac) and the low-resolution slit of the Thermo Fisher Scientific Neptune. The bracketing standard technique was applied to calculate the δ^{25}Mg and δ^{26}Mg values (‰). Each delta value comprises a sequence of 5 repetitions of sample measurements representing 250 ratios (each ratio consists of 4.194 s integration time and 3.0 s idle time). The internal precision of each sequence is given as ±2σ. As standard reference material the DSM3 (Dead Sea Magnesium) was chosen (Galy et al., 2003; Young and Galy, 2004). For further details on the analytical methods please refer to Immenhauser et al. (2010). In order to test the repeatability of Mg isotope measurements, five samples of a carbonate standard RUB (Solnhofer Plattenkalk) were analysed. Each sample was digested, subsequently processed on a different ion exchange column and finally measured resulting in a δ^{26}Mg value of −3.66‰±0.06 2σ.

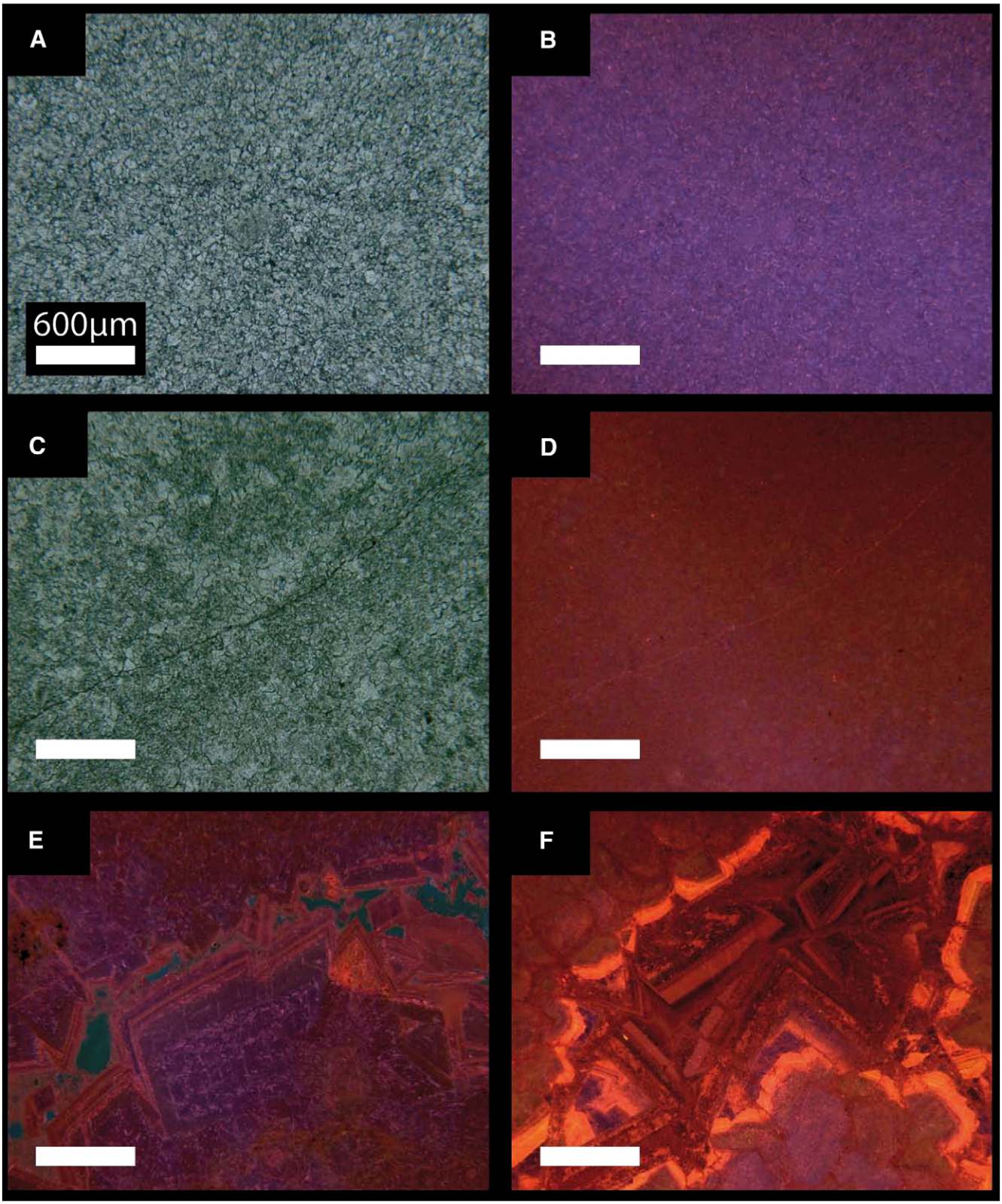

Fig. 4. Photomicrographs of representative thin sections. Scale (600 µm) applies to all images. A) Hauptdolomit dolomicrite D2 phase from Osterhorn Block representing a temperature range of about 100 °C. B) Same as A) but under cathodoluminescence. C) Dolomicrite D2 phase from Kalkkögel representing a temperature range of >350 °C. D) Same as C) but under cathodoluminescence. E) Cathodoluminescence photomicrograph of D4 saddle dolomite from Osterhorn Block. F) Cathodoluminescence image of D4 saddle dolomite from Kalkkögel.

The mono elemental solution Cambridge1 was measured repeatedly providing information about the external reproducibility of mass spectrometry. For the time interval 2005 to 2012, the $\delta^{26}Mg_{Cambridge1}$ value is $-2.57‰ \pm 0.06$ 2σ (n = 431). Between 2011 and 2012 $\delta^{26}Mg_{Cambridge1}$ resulted in $-2.58‰ \pm 0.06$ 2σ (n = 92). The total blank for the complete analysis was 10 ng Mg, which represents an average blank to sample ratio of $2 * 10^{-4}$. The standard deviation (2σ) of groups of samples in Fig. 7 and Table 2b is calculated after Taylor (1997).

Table 2a
Hauptdolomit D2 and D4 $\delta^{26}Mg$ and $^{87}Sr/^{86}Sr$ ratios.

Sample	$\delta^{25}Mg$ (‰)	±2σ	$\delta^{26}Mg$ (‰)	±2σ	$^{87}Sr/^{86}Sr$	±2σ
Northern Calcareous Alps, Osterhorn Block						
WiSt1	−0.96	0.01	−1.85	0.01	0.707720	0.000007
WiSt2	−1.00	0.01	−1.92	0.03	0.707831	0.000008
WiSt3	−0.90	0.02	−1.73	0.02	0.708015	0.000007
WiSt8 H*	−0.91	0.02	−1.73	0.05	n.d.	
WiSt9	−0.96	0.02	−1.82	0.03	0.708148	0.000006
WiSt10	−1.03	0.02	−1.98	0.03	0.708097	0.000007
WiSt11	−0.94	0.03	−1.79	0.04	0.707911	0.000007
WiSt12	−0.93	0.02	−1.78	0.03	0.708033	0.000007
WiSt13	−0.96	0.01	−1.86	0.02	0.708013	0.000007
Central Dolomites, Sella massif and Mendel pass						
hdm2	−1.07	0.02	−2.05	0.02	0.707908	0.000006
hds1a	−0.96	0.02	−1.84	0.02	0.707779	0.000006
hdmt1	−0.85	0.01	−1.63	0.03	0.707788	0.000007
hds3	−1.17	0.02	−2.27	0.01	0.708037	0.000007
hds1c	−1.12	0.02	−2.16	0.02	0.707935	0.000006
Sella 2011*	−1.10	0.01	−2.10	0.02	n.d.	
Sella 2011 (2)*	−1.09	0.03	−2.08	0.05	n.d.	
Northern Calcareous Alps, Rellstal						
hdz133	−1.07	0.02	−2.06	0.05	0.707955	0.000006
zi5	−0.99	0.02	−1.92	0.01	0.708058	0.000007
hdz5	−0.73	0.01	−1.41	0.03	0.708115	0.000007
hdz5 leached	−1.00	0.01	−1.93	0.02	n.d.	
zi1	−0.94	0.02	−1.81	0.03	0.708192	0.000006
zi3	−0.78	0.01	−1.50	0.03	0.708336	0.000007
zi3 leached	−0.98	0.01	−1.87	0.02	n.d.	
Central Alps, Piz Lad						
hd1.6	−1.03	0.02	−1.97	0.04	0.708068	0.000007
hdp7	−0.99	0.01	−1.91	0.02	0.708086	0.000006
nk3	−0.91	0.03	−1.73	0.04	0.708564	0.000006
ko1	−1.06	0.01	−2.05	0.01	0.708423	0.000007
hd3.6	−0.95	0.01	−1.84	0.02	0.708132	0.000007
Hda	−1.00	0.02	−1.92	0.04	n.d	
Hd4.6	−1.03	0.02	−1.99	0.03	n.d.	
Central Alps, Kalkkögel						
Hdk2	−0.98	0.03	−1.93	0.03	0.707891	0.000008
Hdk8	−0.97	0.03	−1.85	0.04	0.707851	0.000007
Hdk6	−0.96	0.03	−1.85	0.01	0.707945	0.000006
Hdk6 H*	−1.04	0.03	−2.00	0.02	n.d.	
Hdk7	−0.95	0.02	−1.84	0.05	0.707997	0.000007
Hdk4	−0.94	0.03	−1.81	0.04	0.708043	0.000007
Hdk5	−1.01	0.03	−1.92	0.04	n.d.	
Hdk3	−1.02	0.02	−2.00	0.03	n.d.	

2σ = average of analytical uncertainty for individual samples.
* Hydrothermal saddle dolomite phase D4.

Dolomite $^{87}Sr/^{86}Sr$ ratios indicate the strontium source of burial fluids and alteration effects. Two to six mg of dolomite sample powder was dissolved at 125 °C in PFA-beakers using 1 ml 6 M HCl. The required sample quantity of 500 ng depended on the strontium content of each sample. The samples were dried down and refluxed in 1.5 ml 2.5 M HCl. Before 1 ml of the solution was moved onto quartz glass columns, filled with BioRad ion exchange resin AG50W-X8, the solution was centrifuged for 10 min to partition the insoluble silicate material. The Sr fraction was separated twice according to column calibration pattern. After final evaporation on a hot plate at >100 °C the samples (approximately100 ng Sr) were re-dissolved for mass spectrometry in 1 μl of ionisation enhancing liquid (Birck, 1986) and loaded on Re-filaments. The $^{87}Sr/^{86}Sr$ ratio was determined with a 7 collector Thermal Ionisation Mass spectrometer (TIMS) MAT262 in 3 collector dynamic mode. As standard reference materials NIST NBS 987 and USGS EN-1 were chosen. The total blank for Sr isotope analysis, including chemical separation and loading blank, is 1.5 ng. The repeatability was tested with the USGS EN-1 modern bivalve carbonate, which passed through the identical procedures as all samples. The average $^{87}Sr/^{86}Sr$ value is 0.709160 ± 0.000027 2σ (n = 209). The reproducibility of Sr measurements represented by NBS987, which was directly loaded onto a Re filament, is 0.710240 ± 0.00034 2σ (n = 233). Please refer to Faure and Powell (1972) for details.

In order to define the diagenetic carbon source and the degree of diagenetic alteration of dolomite light stable isotope ratios, carbon and oxygen isotope signatures were analysed from aliquots of samples. For carbon and oxygen isotope analysis, 0.3 ± 0.03 mg dolomite sample material was weight in and analysed on a ThermoFinnigan MAT 253 coupled to a Gasbench II and a PAL auto sampler (GasIRMS). All isotope ratios are reported as per mil (‰) deviation from the Vienna-Pee Dee Formation belemnite (V-PDB) standard. The certified carbonate standards NBS 19, IAEA CO-1 and CO-8 and an internal standard (RUB standard) were used. The standard deviations (2σ) of 9 RUB standards measured within these sample sequences are 0.06‰ and 0.08‰ for C- and O isotopic measurements, respectively.

In order to complement isotope data, major and trace elemental analysis was performed from aliquots of all samples. Approximately 1.5 ± 0.15 mg of the dolomite samples were dissolved in 3 M HNO_3. Afterwards the solution was diluted with 2 ml of deionised H_2O (>18.2 MΩ cm^{-1}). With an inductively coupled plasma optical emission spectrometer (ICP-OES, Thermo Fisher Scientific iCAP 6500 DUO) the concentration of Ca, Mg, Fe, Mn, Sr and Ba of the carbonate samples was measured at the Ruhr-University Bochum. Together with each set of samples, eight samples of certified reference material (BSC-CRM-512, dolomite and BSC-CRM-513, limestone) were determined. All major and trace elemental results are reported in ppm (parts per million) and errors are given as ±%RSD.

4. Data reporting

4.1. Sample characterization

4.1.1. Cathodoluminescence

This study focuses on the earliest diagenetic dolomicrite (D2) and the latest diagenetic saddle dolomite (D4) phase as defined in Zorlu et al. (2007). Dolomite type D2 from sampling locations 1 (Osterhorn Block) and 2 (Dolomite Alps) show a violet-red to pale-red luminescence colour. In contrast, type D2 dolomite from sampling location 5

Table 2b
Hauptdolomit mean $\delta^{26}Mg$ D2/D4 and mean $^{87}Sr/^{86}Sr$ D2 values.

Sampling locality	$\delta^{26}Mg$ min. (‰)	$\delta^{26}Mg$ max. (‰)	$\delta^{26}Mg_{mean}$ (‰) (D2 and D4)	±2σ	$\delta^{26}Mg_{mean}$ (‰) (D2)	±2σ	$^{87}Sr/^{86}Sr$ (D2)	±σ
Northern Calcareous Alps, Osterhorn Block	−1.98	−1.73	−1.83 (n = 9)	0.17	−1.84 (n = 8)	0.16	0.707971 (n = 8)	0.000142
Central Dolomites, Sella massif and Mendel pass	−2.27	−1.63	−2.02 (n = 7)	0.43	−1.99 (n = 5)	0.51	0.707889 (n = 5)	0.000108
Northern Calcareous Alps, Rellstal	−2.06	−1.81	−1.92 (n = 5)	0.19	−1.92 (n = 5)	0.19	0.708131 (n = 5)	0.000143
Central Alps, Piz Lad	−2.05	−1.73	−1.91 (n = 7)	0.21	−1.91 (n = 7)	0.21	0.708255 (n = 5)	0.000225
Central Alps, Kalkkögel	−2.00	−1.81	−1.89 (n = 8)	0.14	−1.88 (n = 7)	0.12	0.707945 (n = 5)	0.000075
All data	−2.27	−1.63	−1.91 (n = 36)	0.23	−1.91 (n = 32)	0.24	0.809201 (n = 28)	0.000188

2σ = two standard deviations of $\delta^{26}Mg$ values for the group of samples (Taylor, 1997).

(Kalkkögel) is characterized by a wine-red luminescence colour (Fig. 4). Saddle dolomite (D4) is characterized by a shift from violet-red luminescence in samples from sampling location 1 and 2 to dark red in samples from sampling location 5 (Fig. 4).

Fig. 5 shows a transmitted light- and luminescence photomicrograph in combination with three luminescence-spectra measured on dolomicrite D2 and saddle dolomite D4 of sampling location 2 (Dolomite Alps, Sella and Mendel). The peak maxima of luminescence-spectra of dolomicrite D2 increase from 649 to 650 nm in sampling locations 1 and 2 to 652–654 nm in sampling locations 3 through 5 (Fig. 6A, Table 5). The peak maxima of luminescence-spectra of saddle dolomite of all sampling locations range between 647 and 653 nm (Fig. 6A, Table 5).

4.1.2. Crystal structure

The two dolomite phases investigated show a wide range in the degree of order [R = I (015/110)], that varies from 0.29 to 1.03 (Table 5, Fig. 6B). Specimen from sampling location 5 (Kalkkögel) are characterized by a high degree of order 0.87 (n = 5), whereas dolomites from sampling location 1 (Osterhorn Block) have a low degree of order of 0.37 (n = 8). The $d_{(104)}$ values of dolomite phases D2 and D4 range from 2.903 Å to 2.880 Å (Table 5, Fig. 6B). Dolomite samples from sampling location 1 (Osterhorn Block) show the highest $d_{(104)}$ values. The degree of order and the $d_{(104)}$ values correlate positively (Fig. 6B). The mean $CaCO_3$ content decreased from 53.5 mol% (sampling location 1) to 49.3 mol% (sampling location 5; Table 5).

4.2. Geochemical results

4.2.1. Magnesium isotopes ($\delta^{26}Mg$)

Table 2a/b and Fig. 7 provide an overview of all dolomicrite D2 and hydrothermal D4 dolomite $\delta^{26}Mg$ data. Mean data characteristics are summarized below: The mean $\delta^{26}Mg$ ratios of all samples range from -1.83 ± 0.17‰ 2σ (n = 9) (sampling location 1, Osterhorn Block), -2.02 ± 0.43‰ 2σ (n = 7) (sampling location 2, Dolomite Alps, Sella and Mendel), -1.92 ± 0.19‰ 2σ (n = 5) (sampling location 3, Rellstal), to -1.91 ± 0.21‰ 2σ (n = 7) (sampling location 4, Piz Lad) and -1.89 ± 0.14‰ 2σ (n = 8) (sampling location 5, Kalkkögel; Fig. 7). Magnesium isotope data of samples from the sampling location 2 representing two sampling areas (Mendel pass and Sella massif), shows the broadest variation of all sample locations (±0.43 2σ) and is equivalent to diagenetic fluid temperatures of 100 °C. Sampling locations 1 and 3 are characterized by intermediate two standard deviations (±0.17 to ±0.212σ). The smallest range in magnesium isotopic composition is found for sampling location 5 (±0.142σ) (Kalkkögel; Fig. 7).

Magnesium isotope ratios of saddle dolomites (D4) correlate with the $\delta^{26}Mg$ dolomicrite (D2) values (Fig. 7). The hydrothermal dolomites (D4) are represented by four $\delta^{26}Mg$ data points. One data point from sample region 1 with a $\delta^{26}Mg$ value of -1.73 ± 0.05‰ 2σ conspicuously deviates from the other data that have a mean value of -2.06 ± 0.34‰ 2σ (n = 3) (Fig. 7).

4.2.2. Strontium isotopes ($^{87}Sr/^{86}Sr$)

Dolomite (D2) $^{87}Sr/^{86}Sr$ ratios (Table 2a/b and Fig. 8) range between 0.707720 (sampling location 1, Osterhorn Block) and 0.708564 ± (sampling location 3, Piz Lad). The mean $^{87}Sr/^{86}Sr$ value of all dolomicrites D2 is 0.708031 ± 0.000371 $2\sigma_{mean}$ (n = 28). With increasing burial fluid temperature the data scatter decreases from ±0.000132 2σ, n = 13 (sample locations 1 and 2) to ±0.000078 2σ, n = 5 (sample location 5) (Fig. 8).

4.2.3. Oxygen and carbon isotopes ($\delta^{18}O$ and $\delta^{13}C$)

Dolomicrite D2 groups 1 and 2 are characterized by their different $\delta^{18}O$ values as seen in Fig. 9. The $\delta^{18}O$ data of all dolomicrites (D2) range between −7.7‰ and +1.3‰. D2 dolomicites were subdivided in two groups by their more and less pronounced ^{18}O depleted δ values. Group 1 has a mean value of $-1.2‰ \pm 0.03\sigma$ (n = 23; Table 3 and Fig. 9). Five samples yielded ^{18}O-depleted values between −7.7‰ and −4.8‰, referred here to as Group 2 include a mean value of $-6.7‰ \pm 0.03\sigma$, (n = 5); Table 3, Fig. 9. Similarly, hydrothermal saddle D4 dolomites are equally depleted (−7.9‰ to −5.3‰, mean = $-6.4‰ \pm 0.03\sigma$, (n = 4); Fig. 9).

The $\delta^{13}C$ values of dolomicrite D2 samples range from +0.4‰ to +3.6‰ (mean = $+2.2‰ \pm 0.02\sigma$, n = 28; Table 3, Fig. 9). Hydrothermal D4 saddle dolomite $\delta^{13}C$ values range between +1.8‰ to +2.6‰ (mean = $+2.3‰ \pm 0.02\sigma$, n = 4).

The data scatter of the stable isotopes decreases with increasing diagenetic overprint with a threshold limit at about 200 °C (Fig. 10). At the same time, the mean carbon and oxygen values tend to more enriched values for oxygen (−3.2 to −2.1‰) and for carbon (+2.0 to +2.4‰; Fig. 10).

4.2.4. Major and trace element content

Table 4 and Fig. 11 summarise major and trace elemental abundances of all dolomicrites. The mean Mg content of type D2 dolomicrites rises continuously from 113,755 (sampling location 1; ~100 °C) to 125,020 ppm (mean = 118,442 ± 0.3%RSD, x = 28) (sampling location 5; ~350 °C; Fig. 11) ($R^2_{Mg} = 0.89$). Conversely, Ca abundances decrease with increasing Mg abundances from mean values of 218,917 to mean values of 210,050 ppm (mean = 215,311 ± 0.2%RSD, x = 28) between sampling locations 1 and 5 ($R^2_{Ca} = 0.80$). The mean iron contents also decrease (excluding one data point) and range from 121 ppm to 93 ppm (strontium; mean = 123 ± 1.3%RSD, x = 28) and 677 ppm to 232 ppm (iron; mean = 513 ± 1.1%RSD, x = 28) with increasing burial temperature ($R^2_{Fe} = 0.70$). The manganese content is rather invariant and fluctuates non-systematically between 14 and 24 ppm (mean = 21 ± 1.0%RSD, x = 28). Similarly, strontium and manganese are not correlated or anti-correlated ($R^2_{Sr} = 0.25$; $R^2_{Mn} = 0.04$) with temperature and are generally low (Fig. 11).

Patterns in D4 phase saddle dolomite major and trace element contents are rather similar to those described for D2 dolomicrites above (Fig. 11, Table 4). The saddle dolomite sample from sampling location 5 (Kalkkögel) is conspicuously enriched in iron (2261 ppm) and manganese (57 ppm). Mean D2 Mg/Ca molar ratios increased during increasing diagenesis from 0.84 ± 0.12 2σ, n = 8 (sampling location 1) to 0.98 ± 0.01 2σ, n = 5 (sampling location 5) with a sharp rise of cation ordering and reduced data scatter at temperatures above a threshold of approximately 250 °C (Fig. 12). The Mg/Ca molar ratios of saddle dolomites (D4) range between 0.94 and 0.96.

5. Interpretation and discussion

5.1. Open versus closed system behaviour: assessing Hauptdolomite sabkha pore water versus burial fluid geochemical properties

Magnesium isotope ratios in carbonates undergo significant fractionation between fluid and solid (Galy et al., 2002; Carder et al., 2005; Hippler et al., 2009; Immenhauser et al., 2010; Wombacher et al., 2011; Li et al., 2012; Riechelmann et al., 2012; Saulnier et al., 2012). Therefore, $\delta^{26}Mg_{dolomicrite}$ is no direct proxy for $\delta^{26}Mg_{seawater}$ unless this fractionation factor is quantified. One of the perhaps best constrained proxy sets shown here is the strontium isotope data (Fig. 8). This makes strontium a reasonable starting point for any

Fig. 5. A) Cathodoluminescence photomicrographs and B) transmitted light photomicrograph of sample from Dolomite Alps, Sella massif (Sella 2011 a) and C) CL-spectra of a) Hauptdolomit dolomicrites (D2), b) pale saddle dolomites (D3) and c) dark saddle dolomites (D4).

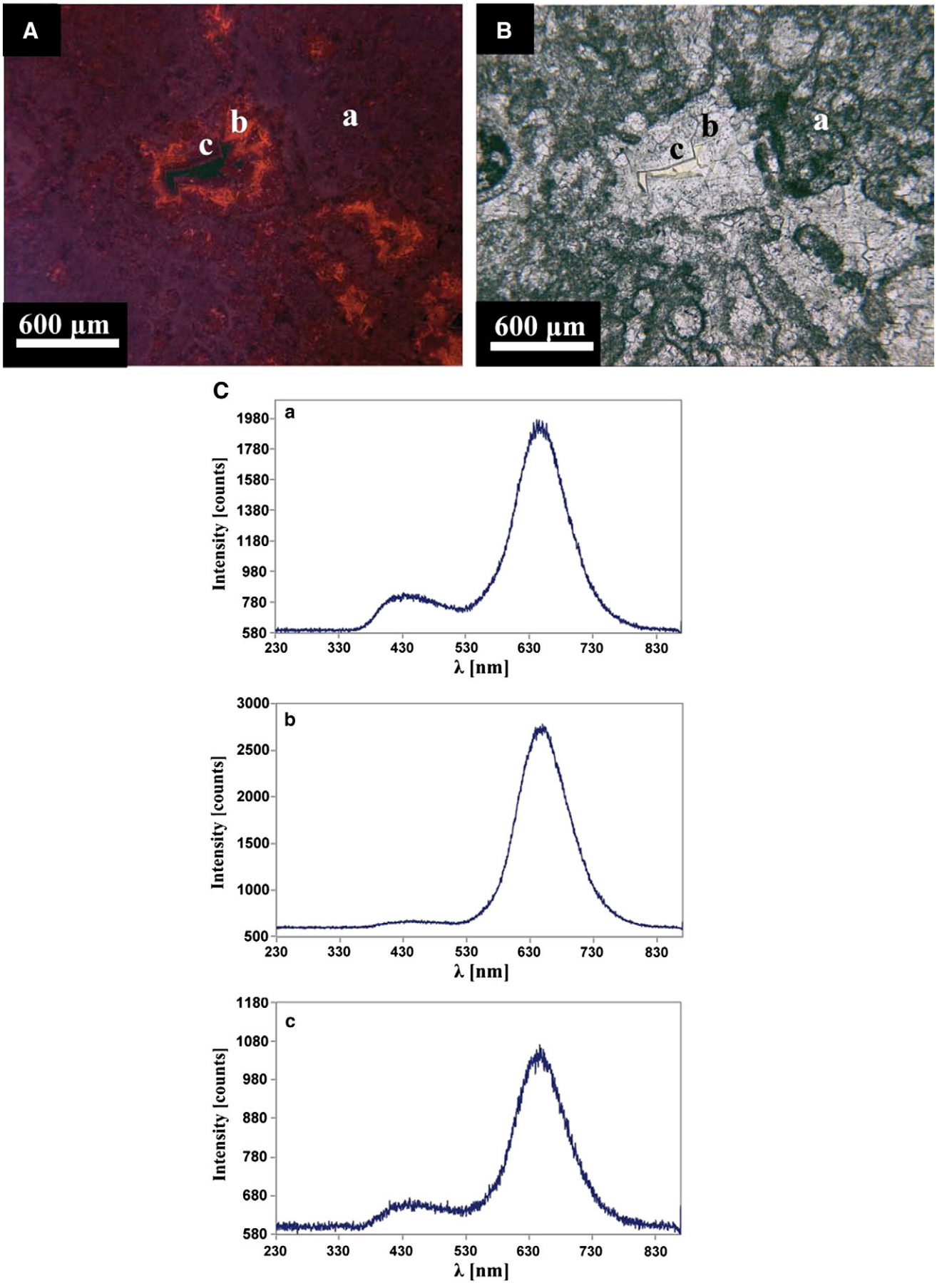
A
a
b
c
600 µm
B
a
b
c
600 µm
C
a
Intensity [counts]
1980
1780
1580
1380
1180
980
780
580
230
330
430
530
630
730
830
λ [nm]
b
Intensity [counts]
3000
2500
2000
1500
1000
500
230
330
430
530
630
730
830
λ [nm]
c
Intensity [counts]
1180
1080
980
880
780
680
580
230
330
430
530
630
730
830
λ [nm]

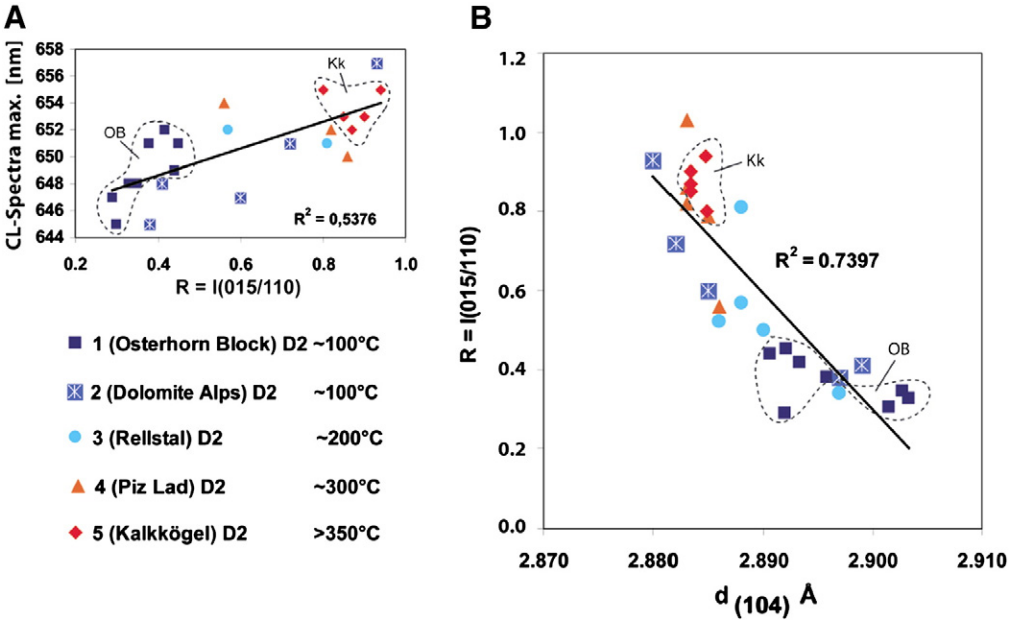

Fig. 6. A) Peak maxima of luminescence spectra (peak position of Mn^{2+}) of Hauptdolomit dolomicrites in nanometres (nm) plotted versus degree of order. B) Degree of order R = I(015)/(110) versus dolomite main peak d_{104} [Å] (dashed line mark Osterhorn Block sampling locality, OB and Kalkkögel sampling locality, Kk).

Table 3
Hauptdolomit D2 and D4 carbon and oxygen isotopic composition.

Sample	$\delta^{13}C$ (‰)	±σ	$\delta^{18}O$ (‰)	±σ
Northern Calcareous Alps, Osterhorn Block				
WiSt1	2.0	0.01	−6.6	0.03
WiSt2	2.1	0.02	−7.5	0.04
WiSt3	1.9	0.01	−2.7	0.03
WiSt9	1.7	0.02	−2.3	0.02
Wist8 H[a]	1.8	0.02	−7.9	0.02
WiSt10	2.0	0.02	−0.7	0.03
WiSt11	1.8	0.01	−4.8	0.02
WiSt12	2.0	0.03	−2.0	0.04
WiSt13	1.9	0.02	−1.8	0.03
Central Dolomites, Sella massif and Mendel pass				
hdm2	3.2	0.01	−1,0	0.03
hds1a	2.2	0.01	−7.7	0.02
hdmt1	1.2	0.02	1.3	0.02
hds3	0.4	0.02	−0.5	0.04
hds1c	1.9	0.03	−2.6	0.02
Sella 2011[a]	2.3	0.02	−6.4	0.02
Sella 2011 (2)[a]	2.6	0.03	−6.1	0.04
Northern Calcareous Alps, Rellstal				
hdz133	3.3	0.03	−0.3	0.02
zi5	1.6	0.01	−0.0	0.02
hdz5	2.0	0.03	−1.9	0.03
zi1	2.1	0.01	−1.2	0.03
zi3	1.6	0.02	0.1	0.04
Central Alps, Piz Lad				
hd1.6	2.8	0.02	−1.0	0.04
hdp7	3.6	0.02	−0.5	0.03
nk3	2.3	0.01	−2.5	0.03
ko1	2.7	0.02	−6.9	0.02
hd3.6	3.1	0.03	−2.4	0.03
Central Alps, Kalkkögel				
Hdk2	2.7	0.02	−1.3	0.04
Hdk8	2.6	0.03	−1.4	0.03
Hdk6	2.2	0.02	−0.7	0.03
Hdk6 H[a]	2.6	0.02	−5.3	0.02
Hdk7	2.7	0.02	−0.2	0.04
Hdk4	1.4	0.02	−1.0	0.03

[a] Hydrothermal saddle dolomite phase D4.

Table 4
Hauptdolomit D2 and D4 major and trace element contents.

Sample	Ca [ppm]	Mg [ppm]	Sr [ppm]	Fe [ppm]	Mn [ppm]	Mg/Ca [mol/mol]
Northern Calcareous Alps, Osterhorn Block						
WiSt1	213,850	118,800	48	157	11	0.92
WiSt2	214,630	119,000	76	283	11	0.91
WiSt3	219,750	111,900	111	627	14	0.84
WiSt9	221,890	107,900	142	1422	26	0.80
WiSt8H[a]	219,530	125,400	60	63	15	0.94
WiSt10	226,260	120,700	185	756	17	0.88
WiSt11	212,820	104,100	56	821	14	0.81
WiSt12	221,010	105,500	132	986	15	0.79
WiSt13	226,470	102,900	189	909	19	0.75
Central Dolomites, Sella Massif and Mendel pass						
hdm2	208,050	122,700	89	535	22	0.97
hds1a	225,070	114,100	47	243	45	0.84
hdmt1	212,120	124,100	64	210	53	0.96
hds3	227,240	104,900	258	1445	28	0.76
hds1c	218,770	115,000	168	619	17	0.87
Sella 2011[a]	214,470	122,300	56	508	30	0.94
Sella 2011 (2)[a]	218,840	125,100	43	384	30	0.94
Northern Calcareous Alps, Rellstal						
hdz133	228,010	110,900	384	889	22	0.80
zi5	212,580	121,500	104	543	17	0.94
hdz5	218,630	116,800	129	699	20	0.88
zi1	221,400	114,200	157	588	14	0.85
zi3	209,500	114,000	128	935	20	0.90
Central Alps, Piz Lad						
hd1.6	210,930	124,500	90	79	10	0.97
hdp7	211,850	122,800	114	183	14	0.96
nk3	206,950	123,600	103	639	13	0.98
ko1	210,950	124,400	74	187	25	0.97
hd3.6	209,570	125,700	85	74	12	0.99
Central Alps, Kalkkögel						
Hdk2	212,600	126,600	89	151	26	0.98
Hdk8	210,000	124,900	105	125	22	0.98
Hdk6	210,650	124,500	103	174	21	0.97
Hdk6H[a]	214,940	125,500	84	2261	57	0.96
Hdk7	210,460	124,800	99	167	15	0.98
Hdk4	209,520	124,300	98	622	32	0.98

Mg/Ca = mol/kg/mol/kg.
[a] Hydrothermal D4 phase saddle dolomite.

Table 5
X-ray diffraction analysis of Hauptdolomit samples, including dolomite main peak at d_{104} [Å], $CaCO_3$ content [mol%], peak maxima of luminescence spectra (Mn^{2+} position) [nm] and degree of order (R).

Sample	d(104)Å	Mol% $CaCO_3$	Peak max. Cl-spectra [nm]	R = I(015/110)
Northern Calcareous Alps, Osterhorn Block				
WiSt1	2.893	52.33	652	0.42
WiSt2	2.891	51.67	649	0.44
WiSt3	2.896	53.33	651	0.38
WiSt9	2.903	55.67	648	0.33
WiSt10	2.902	55.33	645	0.30
WiSt11	2.892	52.00	651	0.45
WiSt12	2.903	55.67	648	0.35
WiSt13	2.892	52.00	647	0.29
Central Dolomites, Sella massif and Mendel pass				
hdm2	2.885	49.67	647	0.60
hds1a	2.882	48.67	651	0.72
hdmt1	2.880	48.00	657	0.93
hds3	2.897	53.67	645	0.38
hds1c	2.899	54.33	648	0.41
Northern Calcareous Alps, Rellstal				
hdz133	2.897	53.67	n.d.	0.34
zi5	2.888	50.67	651	0.81
hdz5	2.886	50.00	n.d.	0.52
zi1	2.890	51.33	n.d.	0.50
zi3	2.888	50.67	652	0.57
Central Alps, Piz Lad				
hd1.6	2.883	49.00	652	0.82
hdp7	2.886	50.00	654	0.56
nk3	2.885	49.67	n.d.	0.79
ko1	2.883	49.00	650	0.86
hd3.6	2.883	49.00	n.d.	1.03
Dolomites, Kalkkögel				
Hdk2	2.885	49.60	655	0.80
Hdk8	2.883	49.13	652	0.87
Hdk6	2.883	49.13	653	0.90
Hdk7	2.885	49.57	655	0.94
Hdk4	2.883	49.13	653	0.85

discussion regarding Triassic sabkha pore fluid geochemistry. Having said this, it must be emphasized that the regionally very expansive Hauptdolomit sabkha environment of the Triassic world (Müller-Jungbluth, 1970; Zankl, 1971; Bechstädt and Mostler, 1976; Brandner and Resch, 1981; Dercourt et al., 1993; Budd, 1997) is without genuine analogue in modern evaporitic environments. Consequently, any statement regarding the Triassic sabkha pore fluid geochemistry must remain, to some degree, speculative.

5.1.1. Dolomite $^{87}Sr/^{86}Sr$ ratios

Dolomite $^{87}Sr/^{86}Sr$ ratios of marine carbonate minerals characterize the diagenetic fluid with regard to strontium source and alteration effects during diagenesis, dolomitization and regional metamorphism (Faure, 1977). The $^{87}Sr/^{86}Sr$ ratios represent a mixing of different strontium sources characterized by different initial strontium isotopic compositions. This is in agreement with the work of Banner (1995), predicting homogeneous equilibrium, where the Sr isotope ratio in the solid and the fluid phase is the same.

According to Veizer et al. (1999) and Korte et al. (2003) the $^{87}Sr/^{86}Sr$ ratio of Triassic seawater is in the order of 0.7076 to 0.7081. Along similar lines, Koepnick et al. (1990) proposed values of 0.7075 to 0.7080. Dolomicrite D2 $^{87}Sr/^{86}Sr$ ratios (Table 2a) are in good agreement with these data. From this, it is tentatively suggested that Hauptdolomit D2 dolomicrites preserved the $^{87}Sr/^{86}Sr$ ratio of the evaporated Triassic sabkha pore water from which dolomites precipitated. In contrast, the Hauptdolomit D3 and D4 $^{87}Sr/^{86}Sr$ ratios deviate clearly from Triassic marine values pointing to open system diagenesis and hydrothermal pore fluids (Zorlu (2006, 2007; D3 = 0.708302–0.708999; D4 = 0.719377). Having said this, we acknowledge that some examples of dolomicrites elsewhere were probably precipitated from mixed marine-meteoric waters at near-surface conditions and yet, these dolomicrites still retain their primary Sr-isotope signatures (Conliffe et al., 2009). Given the clear evidence for a Sabkha type dolomite precipitation in the case of the Hauptdolomit (Frisia, 1994; Iannace and Frisia, 1994), however, the authors favour the interpretation of an evaporated Triassic sabkha pore water strontium signature.

5.1.2. Dolomite oxygen and carbon isotope ratios

Case studies of present-day evaporitic settings such as those of Delaygue et al. (2000), Zeebe (2001) and Benway and Mix (2004), for example, reported that increasing sea water salinity and pH value leads to ^{18}O enriched δ_{sw} values (‰$_{SMOW}$). Accordingly, McKenzie (1981) proposed $\delta^{18}O_{SMOW}$ values of +2.68 to +5.58‰ for modern pore-fluids in the coastal sabkha of Abu Dhabi. In contrast, the oxygen isotopic composition of Triassic seawater ranges between −1.5 to −2.3‰ SMOW (Veizer et al., 1999). Sabkha pore fluids, from which the proto-dolomites precipitated, were most likely evaporated and thus characterized by considerably elevated salinities affecting seawater $\delta^{18}O$ values. Some dolomicrites (D2) oxygen isotope ratios are consistent with published Triassic marine carbonate values (−1.1 to

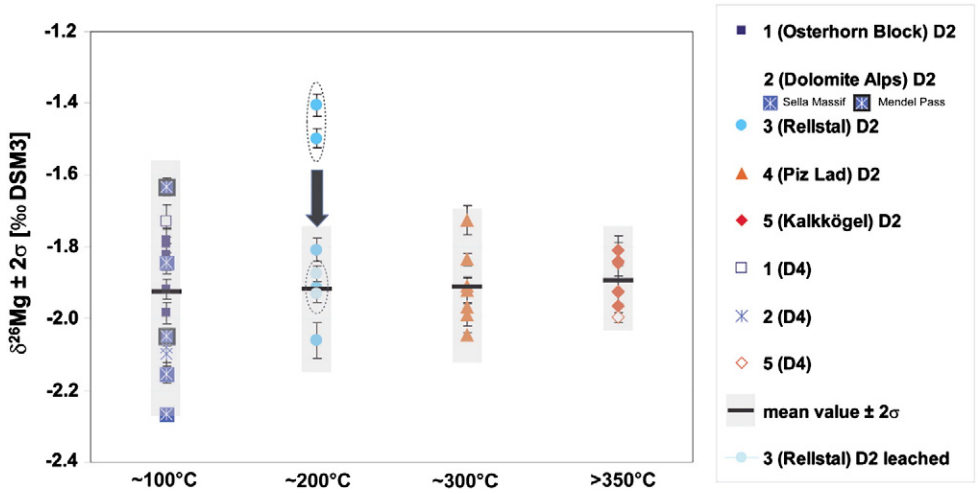

Fig. 7. Magnesium isotopic composition of D2 and D4 phase Hauptdolomit as a function of increasing burial temperatures (dashed line mark changing $\delta^{26}Mg$ values after leaching aliquots). Black lines within light grey squares represent the $\delta^{26}Mg$ mean values and standard deviations of the different group of samples (sampling locations). The standard deviation (2σ) is defined after Taylor (1997). In addition, the average of analytical uncertainty is shown for every sample.

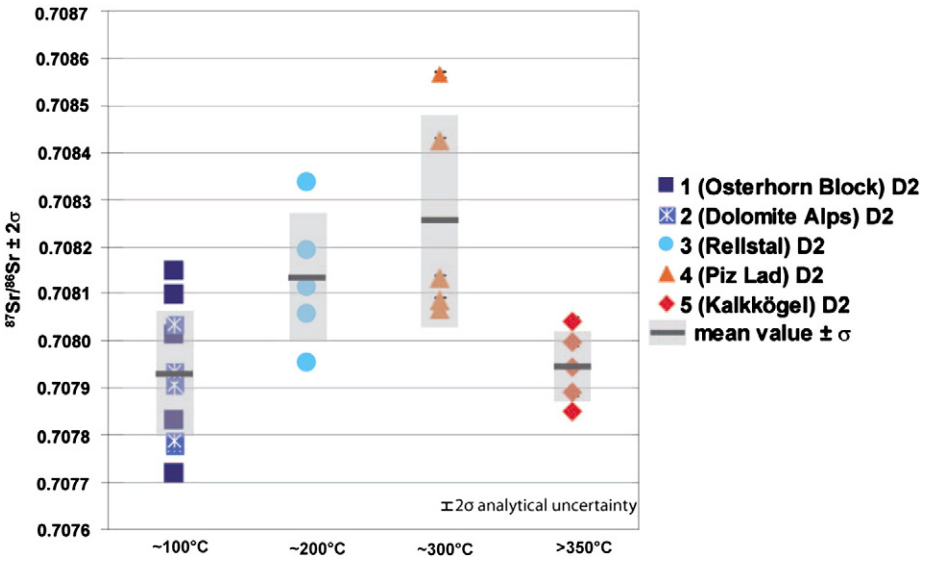

Fig. 8. Strontium $^{87}Sr/^{86}Sr$ isotope data of Hauptdolomit dolomicrites D2 plotted against burial temperature. Black lines within light grey squares represent the $^{87}Sr/^{86}Sr$ mean values and standard deviations of the different group of samples (sampling locations). The standard deviation (σ) is defined after Taylor (1997). In addition, the average of analytical uncertainty (2σ) is shown for every sample.

−4.3‰; Veizer et al., 1999). Applying the dolomite–calcite correction factor $\Delta^{18}O_{Dol-Calcit}$ of +3‰ (Budd, 1997), the $\delta^{18}O$ values for best preserved Triassic dolomites would result in a range of −1.3 to +1.9‰ (Fig. 9). The majority of Hauptdolomit $\delta^{18}O$ values are more depleted, particularly the D4 phase, resulting in an overall mean value of −1.8‰ ± 0.03σ (n = 28; Fig. 9).

Given that the commonly warm to hot burial fluid is the main source of diagenetic oxygen (Dickson and Coleman, 1980; Lohman, 1988), dolomicrite D2 and saddle dolomite D4 $\delta^{18}O$ reflect a semi-closed diagenetic system with a strong diagenetic temperature signal rather than an evaporation signal or an unspecified admixture of both factors. In addition, the $\delta^{18}O$ mean values slightly increase with increasing diagenesis from −3.2‰ to −2.1‰ ($R^2 = +0.08$) (Fig. 9). Dolomicrite D2 oxygen isotope values have been subdivided in what is here labelled group 1 and group 2, respectively. Each group is characterized by its specific $\delta^{18}O$ ratios (Fig. 8). According to Gregg and Sibley (1984), idiotopic planar crystal boundaries found in D2 dolomicrites are indicative of precipitation temperatures below 50 °C, whilst xenotopic D4 saddle dolomites with non-planar boundaries result from elevated temperatures greater than 50 °C.

Applying the work of Land (1985), the paleo-temperatures of dolomite precipitation from a fluid with a Triassic–Norian $\delta^{18}O_{SMOW}$ value of −0.5‰ (Lohman, 1988) were calculated as an independent test. In the case of dolomicrite D2-group 1 and saddle dolomite D4, the outcome of this calculation is in agreement with the proposed critical roughening temperature boundary of 50–60 °C (Dolomicrite D2-group 1: D2 = 39 °C; D4 = 71 °C). Dolomicrite D2 group 2 data, in contrast, disagree with the critical roughening temperature boundary proposed by Gregg and Sibley (1984). These dolomites reflect higher precipitation temperatures of 73 °C that are not typical for dolomicrites with idiotopic planar morphologies (Shukla, 1986). The reasons for this could be growth-inhibiting effects of the solution or impurities, which stabilize the crystal faces (Gregg and Sibley, 1984).

In the data set shown here, $\delta^{18}O_{D2}$ shifts to less depleted values when plotting sampling site 1 (Osterhorn Block, ~ 100 °C) with respect to sampling site 5 (Kalkkögel, > 350 °C) but the overall pattern, when

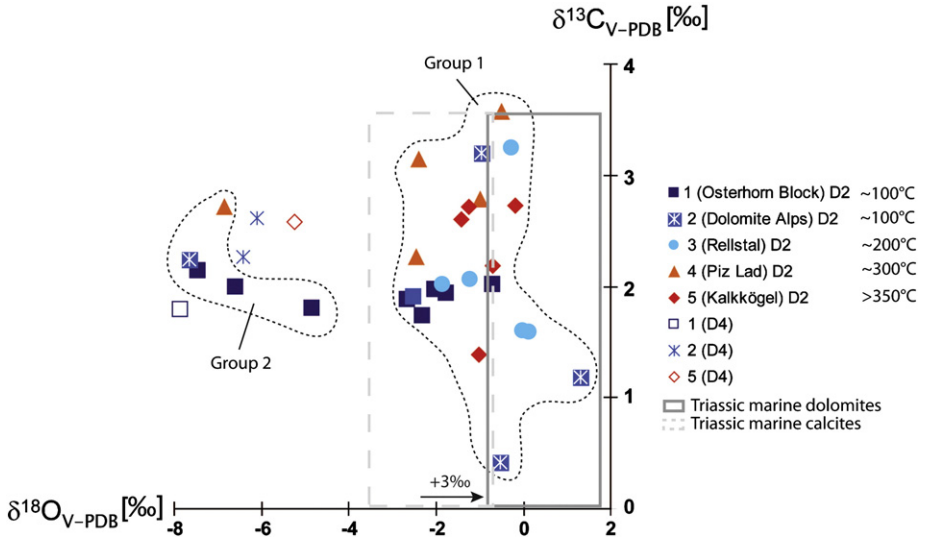

Fig. 9. Carbon and oxygen isotope data of D2 and D4 Hauptdolomit samples from Rellstal, Kalkkögel, Piz Lad, Dolomites and Osterhorn Block sampling localities. Dark grey square represents calculated stable isotope signatures for dolomites precipitated from Triassic seawater ($\Delta^{18}O_{dol-cal} = +3‰$; Budd, 1997). Light dashed square represents the isotopic values of well-preserved calcites/aragonites precipitated from Triassic seawater (Veizer et al., 1999; Korte, 1999).

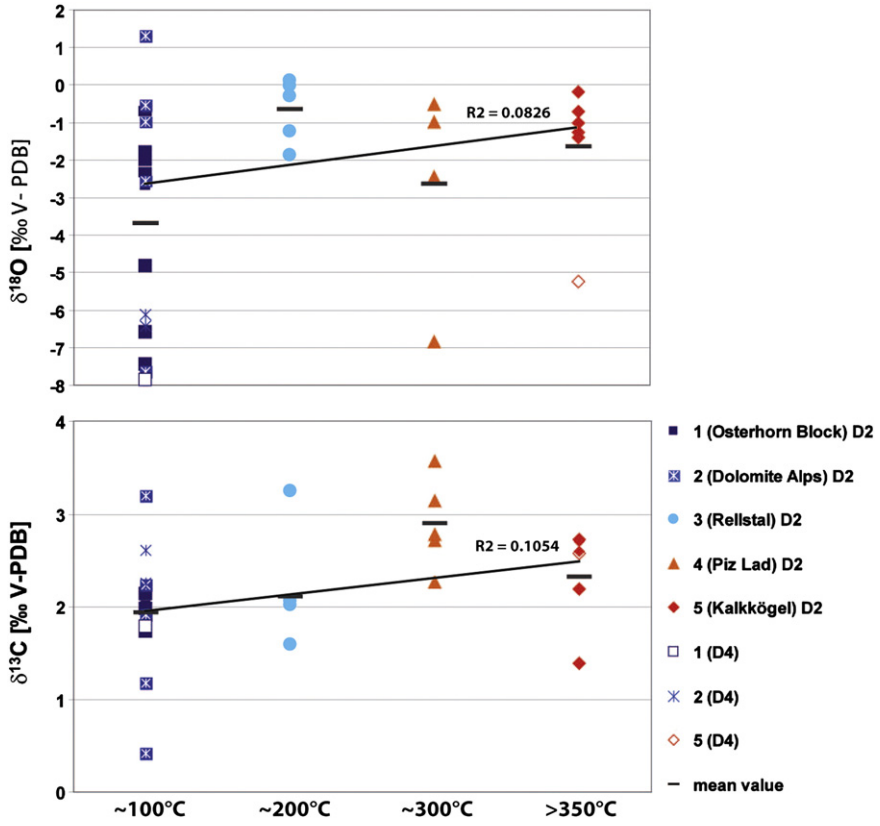

Fig. 10. Hauptdolomit oxygen and carbon isotope data including mean values plotted against burial temperature. Linear curve indicates the correlation between isotopes (D2) and burial temperature. The correlation coefficient is expressed as R^2.

comparing all sampling sites, suggest that a complex series of parameters affected dolomite $\delta^{18}O$ (Fig. 9). Nevertheless, mean $\delta^{18}O_{D2}$ and $\delta^{18}O_{D4}$ values from sampling location 5 (Kalkkögel, >350 °C) are clearly not in agreement with predicted oxygen isotope values that stabilized under these temperatures. Applying the equations of Northrop and Clayton (1966) or Matthews and Katz (1977) approximate $\delta^{18}O$ values of −26 to −27.5‰ result for this temperature range. Given the significantly more positive dolomicrite $\delta^{18}O$ ratios (+1.5 to −8‰; Fig. 9) this implies that dolomite $\delta^{18}O$ was stabilized in a temperature range between 100 and 200 °C. Nevertheless, any assessment of these values is limited due to the most likely non-marine oxygen-isotope signature of Late Triassic sabkha fluids. These considerations are of significance with respect to the dolomicrite magnesium isotope signature.

The data scatter of Hauptdolomit $\delta^{13}C$ data increases (100–300 °C) and then decreases (>350 °C) with increasing diagenesis but to a lesser extent when compared to oxygen isotope ratios. The Hauptdolomit $\delta^{13}C$ data show a narrow range of values (+0.4‰ to +3.6‰, mean = +2.2‰ ± 0.02σ, n = 32; Fig. 9) that agrees with the range of $\delta^{13}C$ values for the best preserved carbonates precipitated from Triassic seawater (+0‰ to +3.6‰; Veizer et al. (1999) and Korte (1999). This suggests that Hauptdolomit dolomicrites preserved their carbon isotopic signature. No clear difference between early diagenetic dolomicrite $\delta^{13}C$ (+2.18‰; n = 28) and burial saddle dolomite $\delta^{13}C$ (+2.31‰; n = 4) is observed. This implies closed system behaviour with Hauptdolomit dolostones being the main source of diagenetic carbon.

5.1.3. Dolomite major and trace elemental geochemistry

Wheeler et al. (1999), using Upper Cenozoic case examples, predicted that Sr concentrations of 50–106 ppm should result for ideal dolomites precipitated from modern seawater (Sr/Ca weight ratio of 0.0195). Strontium concentrations found in D2 dolomicrites are somewhat higher (93–180 ppm), which is in agreement with precipitation from evaporated Triassic sabkha brines (Kranz, 1976). Strontium contents correlate positively with Ca due to the fact that Sr substitutes for Ca in the dolomite structure (Swart and Dawans, 1984). Accordingly, in calcian D2 dolomites from sampling locations 1 and 2, the strontium concentration is higher than in stoichiometric dolomites from sampling location 5.

Modern supratidal dolomites, the proposed analogues to D2 dolomicrites, from the Arabian Gulf, Bahamas and the Florida Keys contain about 300 to 600 ppm of strontium (Behrens and Land, 1972; Land and Hoops, 1973; Bein and Land, 1983). Microbially-induced dolomites are characterized by elevated Sr values of 2800 to 6200 ppm (Sánchez-Román et al., 2011). This implies that Triassic D2 dolomicrites might have lost Sr during diagenesis. Land (1980) suggested that Sr depletion during diagenesis is the consequence of the low distribution coefficient D_{Sr}. This factor, however, is poorly constrained because dolomite has not been synthesized at low (<100 °C) temperatures. Malone et al. (1996) proposed that D_{Sr} varies primarily as a function of the extent of recrystallization, probably due to thermodynamic effects such as variable stoichiometry and, to a lesser extent, cation order of the dolomite. The distribution coefficient D_{Sr} is quantified using the equation of Nernst (1981):

$$D_{Sr} = \left[(Sr/Ca)_{dol}/(Sr/Ca)_{solution}\right]$$

whereby Sr and Ca are commonly weight ratios expressed in molar units [mol/mol]. D_{Sr} between dolomite and its parent fluid was estimated to be in the order of 0.012 at 21 °C by Vahrenkamp and Swart (1990) and values between 0.015 and 0.025 have been suggested by Banner (1995). Mean $(Sr/Ca)_{dol}$ of dolomicrites$_{D2}$ range between 0.00020 and 0.00037. Therefore, a D_{Sr}dol of 0.023 to 0.042 can be calculated for dolomicrites using seawater composition of Sr^{2+} (8 ppm) and Ca^{2+} (411 ppm) (Drever, 1982). These values are more positive compared to the D_{Sr} values of stoichiometric dolomites reported by Vahrenkamp and Swart (1990) and Banner (1995). This might represent evidence

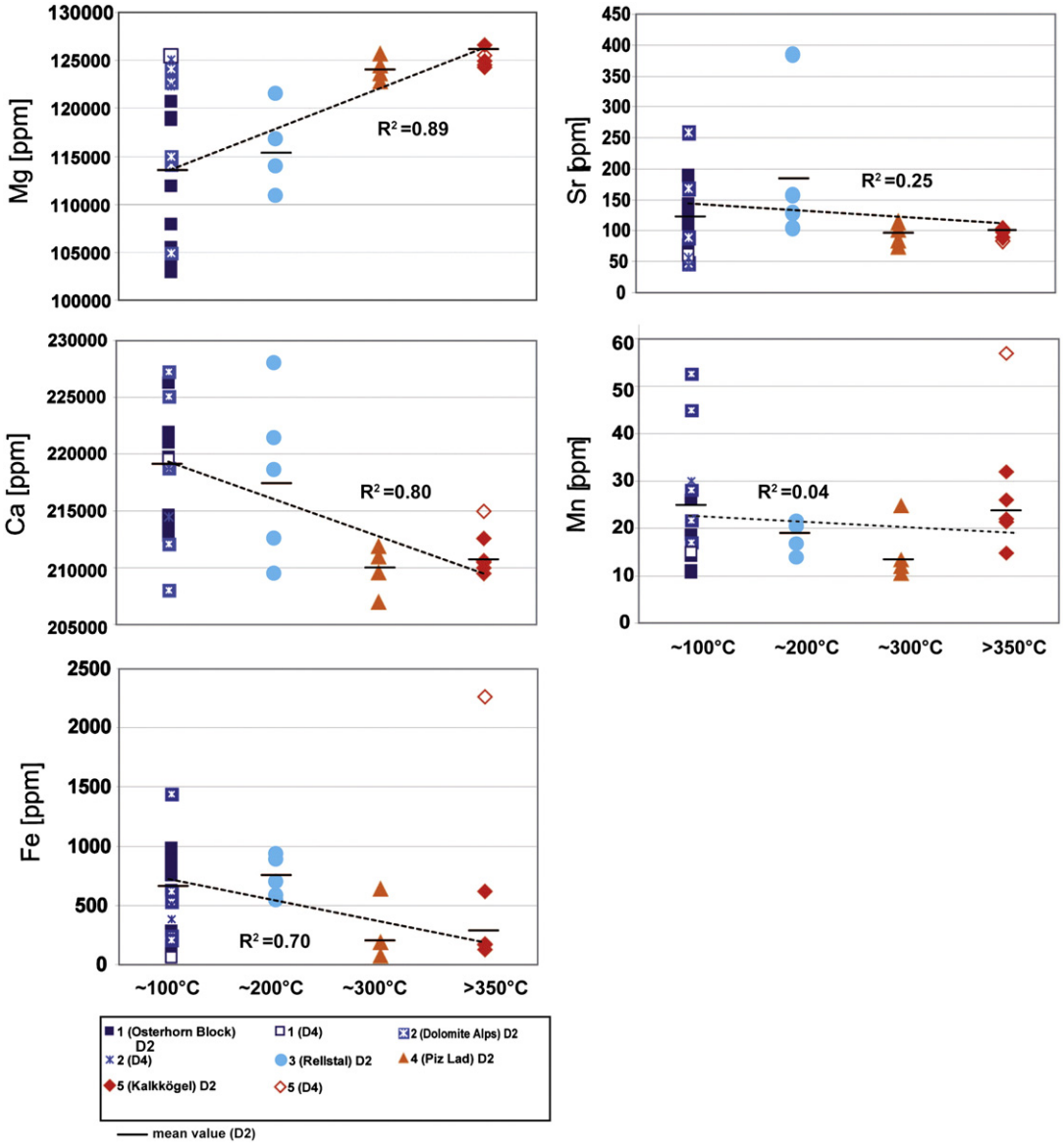

Fig. 11. Hauptdolomit major and trace elemental abundances plotted against burial temperature.

for the elevated salinity of the dolomicrite sabkha parent fluid. The implication of the above discussion for dolomicrite δ^{26}Mg is that D1 (calcian) dolomicrites precipitated from evaporated seawater but then underwent moderate diagenetic alteration during the early diagenetic pathways from D1 to D2 dolomicrite formation, a notion that is in agreement with previous work (Banner, 1995; Zorlu et al., 2007).

Magnesium ions increasingly replace Ca positions in the dolomite crystal structure with increasing stoichiometric order (Nordeng and Sibley, 1993; Kaczmarek and Sibley, 2011). Increasing orders of stoichiometry are linked to increasing temperature, therefore this trend is expected. With progressive diagenetic overprint, the Mg/Ca molar ratio approaches 1. The sharp increase of Mg/Ca molar ratio above a threshold of approximately 250 °C is due to a reorganization of the crystal lattice including a separation of the crystal in Mg-poor calcite and Mg-rich dolomite phase (Richter, 1984; Magdans, 2005).

Calcium was transported in pore fluids and re-precipitated as secondary $CaCO_3$ phase observed in thin sections (Zorlu, 2006). In the D2 dolomicrite samples, that represent diagenetically ordered early precipitates, the influence of burial fluid chemistry on elemental abundances is weak. In contrast, late D4 saddle dolomite from region 5 (Kalkkögel, 350 °C) was precipitated from the burial fluid itself and is enriched in both Fe (2261 ppm) and Mn (57 ppm). The relatively high trace element content is probably temperature-controlled, as temperature affects the distribution coefficient between mineral and fluid (Morse and Bender, 1990; Malone and Baker, 1999). D4 saddle dolomites from sampling locations 1 and 2 are depleted in iron and manganese and represent a low burial temperature correlated with relatively low distribution coefficient. The calcium, iron and strontium content decreases with increasing temperature suggesting diagenetic homogenization of dolomicrites. D4 saddle dolomites show similar major and trace element contents compared to D2 dolomicrites, indicating a closed system reflecting the chemical composition of the surrounding carbonates. The hydrothermal fluid from which the saddle dolomite D4 phase precipitated, was buffered by the surrounding carbonate phases.

5.1.4. Dolomite crystal structure and cathodoluminescence properties

Diagenetic processes that lead to a formation of stoichiometric dolomites include: i) precipitation–dissolution processes (Katz and Metthews, 1977; Gaines, 1980; Land, 1980, 1985) and ii) solid state diffusion (Graf and Goldsmith, 1956). Both of these processes affect the Mg/Ca ratio of the dolomite crystal structure. Frisia and Wenk

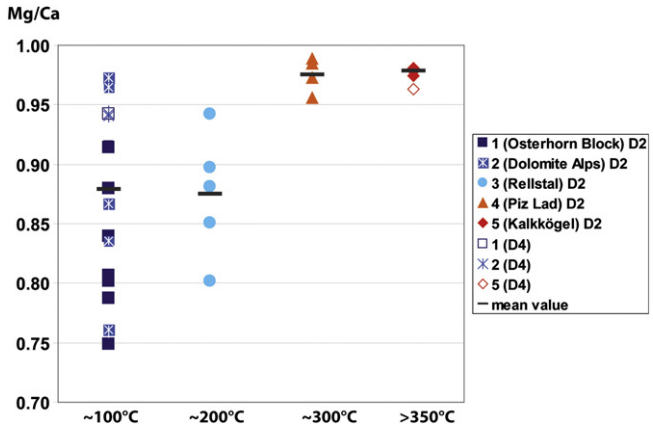

Fig. 12. Hauptdolomit Mg/Ca molar ratios of dolomicrite D2 and saddle dolomite D4.

(1993) published results of a TEM and AEM study with focus of multi-step dolomitization in the Upper Triassic Hauptdolomit. One important observation is that the onset of solid-state diffusion is recorded in some of the void-filling dolomites that precipitated from fluids with temperatures in excess of 60 °C. Based on laboratory experiments, Nordeng and Sibley (1993) and Kaczmarek and Sibley (2011) concluded that high-Mg calcite and calcian dolomite were the first precipitates and only later stoichiometric, ordered dolomite was formed. High-Mg calcite and calcian dolomite progress during dissolution–precipitation reactions by means of the Ostwald's Step Rule (Nordeng and Sibley, 1993). Calcium-rich dolomites are energetically disadvantaged (enthalpy) in respect to well-ordered stoichiometric dolomite (Chai et al., 1995). Solid-state diffusion during dolomitization occurred by diffusion of Mg^{2+} ions into the solid crystal lattice and can be described by the Arrhenius equation (Samtani et al., 2002). In essence, the transformation from poorly ordered calcian dolomite to well-ordered dolomite is controlled by temperature and time. Given a reasonably coeval age of all dolomite samples (~210 Ma), it was mainly temperature that drove dolomite diagenesis. The activation energy must be high enough to accelerate the redistribution process between calcium and magnesium. In the view of the authors, this is mainly a diffusion controlled process.

Under increasing burial fluid temperatures (>250 °C) and with time, stoichiometric and ordered dolomite formed as increasing amounts of Ca in the crystal structure was replaced by Mg (Richter, 1984; Magdans, 2005). The best ordered dolomicrites (D2) are those that experienced burial temperatures of about 350 °C (Fig. 12). In addition, the D4 dolomite phase is nearly stoichiometric even for diagenetic temperature around 100 °C and therefore indicates precipitation from warmer (burial) hydrothermal fluids. Conversely, poorly ordered calcian dolomite (53.5 mol% $CaCO_3$) is found in sampling locations representing peak diagenetic temperatures of 100 °C and less. Therefore, a relation between crystal lattice structure (R; $d_{(104)}$), chemical composition ($CaCO_3$ content) and temperature is observed and the most important thermodynamic and kinetic factors involved have to be considered (Nordeng and Sibley, 1993). High Mg/Ca molar ratios of saddle dolomites (mean: 0.95, n = 4) reflect precipitation from fluids warmer than 60 °C with high salinity (2 to 6 times that of seawater; Radke and Mathis, 1980; Gregg and Sibley, 1984; Machel, 1987; Sibley and Gregg, 1987).

Within the Hauptdolomit crystal structure, Mn^{2+} preferentially occupies Mg^{2+} sites (El Ali et al., 1993; Habermann et al., 1996; Gillhaus et al., 2000, 2001). The shift from the diagenetic domain (sampling locations 1 through 3) to low grade metamorphic one (sampling locations 4 and 5) is documented in the observed changes in luminescence colours in D2 and D4 dolomite phases (Fig. 4). In addition, the peak maxima of the luminescence-spectra shift to higher wavelengths from diagenetic sampling locations (649 nm) to low grade metamorphosis domains (654 nm) due to a progressing change in crystal lattice (Fig. 6A). Increasing stoichiometry is attended by change of luminescence peak maxima to higher wavelengths.

5.2. Hauptdolomit magnesium isotope ratios

5.2.1. Magnesium isotope fractionation between fluid and solid phase

Modern seawater δ^{26}Mg values are in the order of −0.82‰ independent of water depth or geographic location (see references in Hippler et al., 2009) and long $Mg_{seawater}$ residence times of τ ~ 13 Myr were suggested by Broecker and Peng (1982). Hippler et al. (2009) reports seawater data from the Dutch Wadden Sea collected in March to August 2007. These values are from seawater with a 28.0–30.5 psu salinity range and a seasonal temperature range of 7.5 to 19 °C. Individual seawater samples were indistinguishable in terms of their δ^{26}Mg ratios suggesting a very limited impact of both salinity and seawater temperature on magnesium isotope ratios. Ling et al. (2011) investigated 40 seawater samples from the Gulf of Mexico and found a homogenous Mg isotopic composition ($\delta^{26}Mg = -0.832 \pm 0.068$‰) within this confined water body.

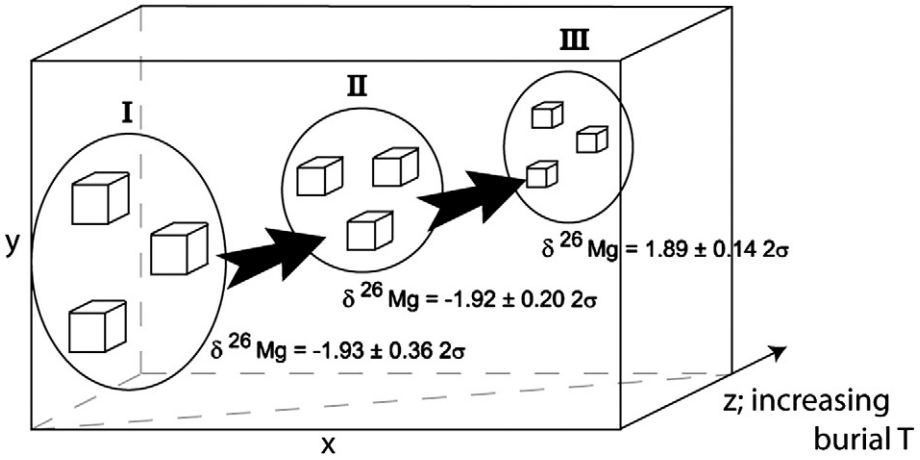

Fig. 13. Conceptual model showing spatial magnesium isotope homogenization with increasing burial temperature for Hauptdolomit D2 dolomicrites. Three-dimensional visualisation (x and y axes denominate space whilst z axis denominates temperature) within sabkha dolomicrite. Magnesium isotope homogenization is indicated by progressively smaller cubes with increasing data scatter. δ^{26}Mg values: I = −1.92 ± 0.32‰ (sampling locations 1 and 2); II = −1.91 ± 0.17‰ (sampling locations 3 and 4); and III = −1.88 ± 0.10‰ (sampling location 5). Pathways I to III are characterized by increasing temperature (I = ~100 °C, II = 200–300 °C, III = >350 °C), volume expansion and increasing Mg isotope exchange. The three dimensional homogenization zone expands with increasing temperature. The latter process increases the rates of the homogenisation process and the isotope exchange. In addition, in pathway I, different sample represents local differences in δ^{26}Mg. Conversely, along pathway III the samples are characterized by nearly homogeneous Mg isotope values.

Magnesium isotope values of inorganic dolomites found in literature vary between −0.8 and −2.4‰ (Galy et al., 2002; Chang et al., 2003; Brenot et al., 2008; Tipper et al., 2008a, 2008b; Wombacher et al., 2009; Jacobson et al., 2010; Pokrovsky et al., 2011), i.e., these values overlap with the analytical results shown here ($\delta^{26}Mg_{meanD2+D4} = -1.91‰ \pm 0.23$ 2σ). The few published data from bacterially mediated recent and sub-recent dolomite $\delta^{26}Mg$ indicate a strong depletion by up to 3‰ relative to the medium from which they precipitated (Carder et al., 2005). In addition, in monospecific laboratory cultures the isotope fractionation is found to vary with bacterial species by up to 1‰ (Carder et al., 2005). With regard to calcite $\delta^{26}Mg$ ratios, published evidence is more substantial. For example, a considerable Mg-isotope fractionation ($1000\ln\alpha_{Mg\text{-}cc\text{-}Mg(aq)} \approx -2.1‰$) was found for abiotic precipitation under laboratory conditions for low-Mg calcite (Immenhauser et al., 2010). Furthermore, Li et al. (2012) published $^{26}Mg/^{24}Mg$ fractionation factors between inorganic Mg-calcite and solution that are changing from −2.70 to −2.22‰ over a temperature range of 4–45 °C.

In summary, data on inorganic Mg-isotope fractionation for the fluid/dolomite system are as yet lacking and the possible impact of evaporated sabkha pore waters on seawater $\delta^{26}Mg$ remains to be tested. A possible way forward is the analysis of present day sabkha dolomites and their respective pore water $\delta^{26}Mg$ signature.

5.2.2. Burial diagenesis: impact on Hauptdolomit crystallinity and $\delta^{26}Mg$ ratios

Temperature is an important physical variable for geochemical processes in terms of isotope fractionation. Further on, the ordering of the dolomite crystal lattice is mainly controlled by temperature and time. Magnesium isotope ratios are coupled to increased crystallinity and Ca–Mg ordering in the dolomite crystal lattice. Applying these principles to the Hauptdolomit magnesium isotope system, the exchange of magnesium (in a fluid or via diffusion) between single crystals in the rock body takes place at increased rates under elevated temperatures.

Magnesium isotope ratios from samples taken at locations 1 and 2 (Osterhorn Block; Dolomite Alps) range between −1.63‰ and −2.27‰ (mean = −1.92‰), whereas data of sampling location 5 (Kalkkögel, 350 °C) vary between −1.81‰ and −2.00‰ (mean = −1.88‰). The average difference between δ-values from sampling locations 1, 2 to 5 thus decreases from 0.43‰ and 0.17‰ to 0.14‰. The highest variability in $\delta^{26}Mg$ (±0.43 2σ) is found in data from sampling location 2 (Central Dolomites, Sella Massif and Mendel pass; Fig. 7). The distance between these two areas is in the order of 50 km. In contrast, samples from sampling location 1 (Osterhorn Block), that equally experienced 100 °C burial temperature, display a much reduced level of $\delta^{26}Mg$ variability (±0.17 2σ). These later samples were collected from the same quarry. The tentative relation between sampling distances within one data set and $\delta^{26}Mg$ variability might suggest that primary and early diagenetic spatial differences in dolomicrite $\delta^{26}Mg$ depend on the local $\delta^{26}Mg$ signal and the degree of spatial isotope homogenization. The latter feature is increasing spatially with increasing burial temperature.

In calcian D1 and D2 dolomites, precipitated from near-surface sabkha fluids, isotope exchange rates are reduced or at least slow and spatially limited. Nevertheless, the homogenization of $\delta^{26}Mg_{D2}$ values goes hand in hand with increasing stoichiometry (Fig. 6) and increasing Mg versus Ca ratios (Fig. 12). Under increasing burial temperature and pressure, increasingly stoichiometric dolomites represent elevated burial diagenetic fluid temperatures resulting in an enhanced rate of magnesium isotope exchange across a given rock volume. A simple model, attempting to explain the progressive homogenization of $\delta^{26}Mg_{D2}$ with increasing temperature is shown in Fig. 13. This model assumes that magnesium exchange between neighbouring rock units takes place at increasing rates along a burial pathway labelled I through III. Pathways I to III are characterized by increasing temperature (I = ~100 °C, II = 200–300 °C, III = >350 °C), volume expansion (three dimensional) and increasing Mg isotope exchange. These observations contrast the often increasing level of isotopic scatter as found for oxygen and carbon isotopes exposed to increasing burial depth and temperature (Bathurst, 1980; Immenhauser et al., 2008; Brand et al., 2010). Therefore, the effect of fluid temperature on magnesium isotope fractionation merits discussion.

Magnesium isotope fractionation is weakly correlated to temperature (Hippler et al., 2009; Rustad et al., 2010; Schauble, 2011), but at fluid temperatures beneath 100 °C fractionation effects are insignificant. Based on precipitation experiments, Li et al. (2012) suggested that the $^{26}Mg/^{24}Mg$ fractionation across the temperature range of +4 °C and +45 °C is temperature dependent and expressed by: $(\Delta^{26}Mg_{cal-sol}) = (-0.158 \pm 0.051) * 106/T2 - (0.74 \pm 0.56)$ (T = Kelvin). At present remains to be tested if the results obtained from magnesian calcites are applicable to (calcian) dolomites.

Nevertheless, the data shown here and in particular the data for D4 stage burial dolomite $\delta^{26}Mg$ ratios, may contribute to a better understanding of these processes. Applying the temperature-related fractionation factors suggested by Galy et al. (2002) and Li et al. (2012) for magnesian calcites to Osterhorn Block (~100 °C) and Kalkkögel D2 phase dolomicrites (~350 °C) results in $\Delta^{26}Mg_{carb-sol}$ −1.88‰ for Osterhorn Block and in −1.15‰ for Kalkögel D2 dolomicrites. Calculated values, as based on magnesian calcites, and, for low temperature, are in agreement with measured values of D2 dolomicrites (Table 2a/b). An additional complication comes from the fact that D2 dolomicrites analysed here have not been precipitated directly from sabkha pore fluids but a D1 precursor stage of calcian sabkha dolomicrites underwent early diagenetic stabilization to the D2 phase progressively overprinted during burial. Burial saddle dolomites D4 show $\delta^{26}Mg$ values (−1.98‰ ± 0.34 2σ, n = 4) that are rather similar (Δ = 0.1‰) to those of early diagenetic D2 dolomicrites (−1.91‰ ± 0.24 2σ, n = 32). This minor difference suggests that temperature-related fractionation factors reported by Li et al. (2012) are probably not applicable to a temperature range above +45 °C and/or may not apply to dolomites in the first place. Thus, we tentatively suggest that temperature fractionation of $\delta^{26}Mg_{dolomite}$ is not significant in a temperature range between 200 and >350 °C (Fig. 7).

Judging from the above discussion, a significant observation is that recrystallization of dolomite and the process of increasing stoichiometric order apparently took place under “closed” system conditions, i.e. in a rock (here Hauptdolomit) buffered system. Magnesium isotope ratios stabilized in a temperature range between 100 and 200 °C (Fig. 7). At 100 °C the Mg isotopic composition found here is similar compared to the calculated values of Schauble (2011). For temperatures exceeding 300 °C, the calculated $\delta^{26}Mg$ values disagree with measured values giving further support to the notion of a host rock buffered system and homogenization of D2 dolomicrites. The magnesium source of the early diagenetic dolomicrites was probably evaporated Triassic sea (sabkha) water and shallow burial pore fluids. Dolomite D4 precipitated from burial fluids under elevated temperatures. This clearly suggests that burial fluids did not carry the ^{26}Mg-enriched signature of silicate rocks (Immenhauser et al., 2010) from stratigraphically deeper levels but mainly that of the Hauptdolomit. This observation is of importance for the burial history of the Hauptdolomit.

In this context, it is of interest that two dolomicrite samples (sampling location 3, Fig. 7) seem to display an open system signature. This is because of their less depleted magnesium isotopic compositions (−1.41‰ and −1.50‰). After treatment of aliquots of these samples with 0.2 M acetic acid in order to remove the easily soluble Mg-calcite/calcite phase the $\delta^{26}Mg$ values of the residue changed to −1.87‰ and −1.93‰ respectively. In conclusion, the calcite phase is enriched in the heavier Mg isotope. This observation is in disagreement with the outcome of theoretical considerations summarized in Rustad et al. (2010) and Schauble (2011). According to these authors, Mg-calcite should be depleted in ^{26}Mg relative to dolomite under isotopic equilibrium conditions, and not enriched. The, at present, perhaps best explanation for

this paradoxical observation is the assumption that in the case studied here, non-equilibrium fractionation processes took place.

5.3. Strengths and weaknesses of the present study and view forward

The data shown here make use of a natural laboratory in the Austroalpine and Southern Alps of Austria and Italy and allow for the direct compilation of an early diagenetic, petrographically homogenous dolomite multi-proxy geochemical record exposed to a well constrained burial gradient. Given that the number of field locations worldwide that allow for such a study is limited, this is clearly a strength of the present data set. Further on, given that early diagenetic dolomicrite D2 and late diagenetic saddle dolomite D4 phases are similar in their magnesium and carbon composition, it was proposed that the Hauptdolomit diagenetic pathways are mainly rock buffered. The implication of this is that dolomite δ^{26}Mg is a conservative proxy even under elevated (low grade metamorphosis) burial temperatures. This is a promising result given the fact that we intend to test the potential of dolomicrite δ^{26}Mg as a potential archive of past marine pore water magnesium isotope signatures.

It must be considered, however, that the stratigraphically very thick and rather uniform Hauptdolomit successions studied here are a very likely case example of a rock buffered system. What needs to be tested is whether stratigraphically thin or locally isolated dolomicrite rock bodies, exposed to differential fluids with differential δ^{26}Mg signatures are geochemically equally conservative. In this sense, it might be worth considering preliminary experimental work using Hauptdolomit rock samples.

Perhaps most important, however, is the quantification of the at present unknown fraction factor between $\delta^{26}Mg_{fluid}$ and $\delta^{26}Mg_{dolomicrite}$. Furthermore, the question if this fractionation factor between sabkha pore water and sabkha dolomicrites is applicable to normal marine seawater precipitation environments needs to be evaluated.

6. Conclusions

1. In five sampling locations, Triassic (Carnian–Norian) D1 calcian, unordered [R = I (015)/(110) = 0.37, n = 8] dolomicrites, precipitated in a spatially extensive sabkha environment, underwent early diagenetic stabilization to increasingly ordered (R = 0.87, n = 5) and increasingly stoichiometric D2 dolomicrites (Mg/Ca > 0.95). D2 dolomicrites and burial D4 saddle dolomites in the same samples record the impact of a burial temperature gradient between about 100 and more than 350 °C.
2. D2 dolomicrite $^{87}Sr/^{86}Sr$ values indicate a well-preserved evaporated Triassic sabkha pore water strontium isotope ratio. In the view of the authors, this supports the notion of an initial proto-dolomite precipitation from evaporated seawater and a very early diagenetic stabilization of phase D2 dolomicrites. This interpretation is supported by clear petrographic evidence for a Triassic Hauptdolomit Sabkha depositional environment allowing for a tentative comparison with well-studied dolomitization processes in modern sabkha settings. Strontium isotope ratios homogenize under increasing burial temperatures.
3. Magnesium (δ^{26}Mg) and carbon (δ^{13}C) are rock buffered and homogenize under increasing burial temperatures. This pattern is most obvious for dolomite δ^{26}Mg ratios ($\delta^{26}Mg_{meanD2} = -1.91‰ \pm 0.03$ 2σ, n = 32; $\delta^{26}{}_{meanD4} = -1.98‰ \pm 0.04$ 2σ, n = 4). Dolomicrite δ^{18}O values reveal a complex multiphase pattern in a semi-closed diagenetic system and stabilization under fluid temperatures between less than 100 and 200 °C.
4. The data shown here represent a first attempt to establish $\delta^{26}Mg_{dolomite}$ as proxies for ancient $\delta^{26}Mg_{seawater}$. Given the long residence time of $\delta^{26}Mg_{seawater}$ τ ~ 13 Myr, this approach is a priori promising. As the dolomicrites studied here were exposed to early diagenetic pore fluid alteration, Hauptdolomit D2 dolomicrite δ^{26}Mg is not a direct proxy for past seawater geochemistry, but rather one for Sabkha evaporated pore-water fluids. Dolomite magnesium-isotope ratios shown here homogenize in a rock buffered system under increasing burial conditions but remain geochemically conservative. Temperature-induced fractionation between fluid and solid is apparently insignificant in the data range between 100 and > 350 °C. A main obstacle for the assessment of these data lies at present in the poor knowledge of fractionation factors between fluid (here evaporated sabkha pore waters) and (calcian) dolomites. An important task for future work is thus the investigation of recent sabkha environments that allow for the sampling and analysis of pore waters and calcian dolomites.

Acknowledgements

The technical staff at Bochum is greatly acknowledged for their assistance in the (non-)traditional isotope and the cathode luminescence laboratory. The German Science Foundation (grant IM 44/7-1) is acknowledged for financial support. Chemical Geology associate editor U. Brand and two anonymous reviewers are greatly acknowledged for detailed and insightful comments.

Appendix A. Supplementary data

Supplementary data to this article can be found online at http://dx.doi.org/10.1016/j.chemgeo.2012.09.014.

References

Anovitz, L.M., Essene, E.J., 1987. Phase equilibria in the system $CaCO_3$–$MgCO_3$–$FeCO_3$. Journal of Petrology 28 (2), 389–415.
Banner, J.L., 1995. Application of the trace element and isotope geochemistry of strontium to studies of carbonate diagenesis. Sedimentology 42, 805–824.
Bathurst, R.G.C., 1980. Deep crustal diagenesis in limestones. Revista del Instituto de Investigaciones Geologicas de la Diputación de Barcelona (Universidad de Barcelona) 34, 89–100.
Bechstädt, T., Mostler, H., 1976. Riff-Becken-Entwicklung in der Mitteltrias der westlichen Nördlichen Kalkalpen. Zeitschrift der deutschen geologischen Gesellschaft 127, 271–289 (Hannover).
Behrens, E.W., Land, L.S., 1972. Subtidal Holocene dolomite, Baffin Bay, Texas. Journal of Sedimentary Petrology 42, 155–161.
Bein, A., Land, L.L., 1983. Carbonate sedimentation and diagenesis associated with Mg–Ca–chloride brines: the Permian San Andreas Formation in the Texas Panhandle. Journal of Sedimentary Petrology 53, 243–260 (Tulsa).
Benway, H.M., Mix, A.C., 2004. Oxygen isotopes, upper-ocean salinity, and precipitation sources in the eastern tropical Pacific. Earth and Planetary Science Letters 224 (3–4), 493–507.
Berástegui, X., Banks, C.J., Puig, C., Taberner, C., Waltham, D., Fernandez, M., 1998. Lateral diapiric emplacement of Triassic evaporites at the southern margin of Guadalquivir Basin, Spain. In: Mascle, A., Puigdefabregas, C., Luterbacher, H.P., Fernandez, M. (Eds.), Cenozic Foreland Basins of Western Europe. Geological Society, London, pp. 49–68.
Birck, J.L., 1986. Precision K–Rb–Sr isotopic analysis: application to Rb–Sr chronology. Chemical Geology 56, 73–83.
Bontognali, T.R.R., Vasconcelos, C., Warthmann, R.J., Bernasconi, S.M., Dupraz, C., Strohmenger, C.J., McKenzie, J.A., 2010. Dolomite formation within microbial mats in the coastal sabkha of Abu Dhabi (United Arab Emirates). Sedimentology 57, 824–844.
Bossellini, A., 1998. Geologie der Dolomiten. Athesia, Bozen.
Brand, U., Azmy, K., Tazawa, J.-I., Sano, H., Buhl, D., 2010. Hydrothermal diagenesis of Paleozoic seamount carbonate components. Chemical Geology 278, 173–185.
Brandner, R., Resch, W., 1981. Reef development in the Middle Triassic (Ladinian and Cordevolian) of the Northern Limestone Alps near Innsbruck, Austria. Special publications. Society of Economic Paleontologists and Mineralogists 30, 203–231 (Tulsa).
Brenot, A., Cloquet, C., Vigier, N., Carignan, J., France-Lanord, C., 2008. Magnesium isotope systematics of the lithologically varied Moselle river basin, France. Geochimica et Cosmochimica Acta 72, 5070–5089.
Broecker, W.S., Peng, T.-H., 1982. Tracers in the Sea. Lamont-Doherty Geological observatory, Colombia University, Palisades, NY 10964 . 690 pp.
Budd, D.A., 1997. Cenozoic dolomites of carbonate islands: their attributes and origin. Earth-Science Reviews 42, 1–47.
Buggisch, W., 1978. Die Grödner Schichten (Perm, Südalpen). Sedimentologische und geochemische Untersuchungen zur Unterscheidung mariner und kontinentaler Sedimente. Geologische Rundschau 67, 149–180.
Buntebarth, G., Stegena, L., 1986. Paleogeothermics — evaluation of geothermal conditions in the geological past. Lecture Notes in Earth Science 5 234 pp.

Burns, S.J., McKenzie, J.A., Vasconcelos, C., 2000. Dolomite formation and biogeochemical cycles in the Phanerozoic. Sedimentology 47 (Suppl. 1), 49–61.
Carder, E.A., Galy, A., McKenzie, J.A., Vasconcelos, C., Elderfield, H.E., 2005. Magnesium isotopes in bacterial dolomites: a novel approach to the dolomite problem. Geochimica et Cosmochimica Acta 69 (10), A213.
Cayeux, L., 1935. Les Roches Sédimentaires de France: Roches Carbonatées. Masson, Paris.
Chafetz, H.S., Rush, P.F., 1994. Diagenetically altered sabkha-type Pleistocene dolomite from the Arabian Gulf. Sedimentology 41 (3), 409–422 (Oxford).
Chai, L., Navrotsky, A., Reeder, R.J., 1995. Energetics of calcium-rich dolomite. Geochimica et Cosmochimica Acta 59 (5), 939–944.
Chang, V.T.-C., Masishima, A., Belshaw, N.S., O'Nions, R.K., 2003. Purification of Mg from low Mg biogenic carbonates for isotope ratio determination using multi-collector ICP-MS. Journal of Analytical Atomic Spectrometry 18, 296–301.
Conliffe, J., Azmy, K., Knight, I., Lavoie, D., 2009. Dolomitization of the Lower Ordovician Watts Bight Formation of the St. George Group, western Newfoundland: evidence of hydrothermal fluid alteration. Canadian Journal of Earth Science 46 (4), 247–261.
De Dolomieu, D., 1791. Sur un genre de pierres calcaires trés peu effervescentes avec les acides et phosphorescentes par la collision. Journal de Physique 39, 3–10.
De Villiers, S., Dickson, J.A.D., Ellam, R.M., 2005. The composition of the continental river weathering flux deduced from seawater Mg isotopes. Chemical Geology 216, 133–142.
Deelman, J.C., 2011. Low-temperature formation of dolomite and magnesite. Geology Series. Compact Disc Publications, Eindhoven, The Netherlands.
Delaygue, G., Jouzel, J., Dutay, J.-C., 2000. Oxygen 18-salinity relationship simulated by an oceanic general circulation model. Earth and Planetary Science Letters 178 (1–2), 113–123.
Dercourt, J., Ricou, L.E., Vrielnyck, B., 1993. Atlas Paleoenvironmental Maps: BEICIP-FRANLAB. IFP, Rueil-Malmaison.
Dickson, J.A.D., Coleman, M.L., 1980. Changes in carbon and oxygen isotope composition during limestone diagenesis. Sedimentology 27, 107–118.
Dietrich, H., 1980. Mineralogisch-petrographische Untersuchungen zur Metamorphose des Brennermesozoikums, Dissertation an der naturwissenschaftlichen Fakultät der Leopold-Franzes-Universität, Innsbruck, 137 pp.
Dietrich, H., 1983. Zur Petrologie und Metamorphose des Brennermesozoikums (Stubaier Alpen, Tirol). Tschermaks Mineralogische und Petrologische Mitteilungen 31, 235–257 (Wien).
Donofrio, D.A., 2008. Kurzmitteilungen zu Conodonten, Echinodermen- und Fischresten aus dem Brennermesozoikum (Kalkkögelgruppe SW Innsbruck, Tirol) und deren Paläotemperaturen. Geography of the Alps 5, 83–95 (Innsbruck).
Dössegger, R., Müller, W.H., 1976. Die Sedimentserien der Engadiner Dolomiten und ihre lithostratigraphische Gliederung. Eclogae Geologicae Helvetiae 69, 229–238 (Basel).
Dössegger, R., Furrer, H., Müller, W.H., 1982. Die Sedimentserien der Engadiner Dolomiten und ihre lithostratigraphische Gliederung (Teil 2). Eclogae Geologicae Helvetiae 75 (2), 303–330 (Basel).
Drever, J.I., 1982. The Geochemistry of Natural Waters. Prentice-Hall, Englewood Cliffs, New Jersey . 388 pp.
El Ali, A., Barbin, V., Calas, G., Cervelle, B., Ramsyer, K., Bouroulec, J., 1993. Mn^{2+}-activated luminescence in dolomite, calcite and magnesite: quantitative determination of manganese and site distribution by EPR and CL-spectroscopy. Chemical Geology 104, 189–202 (Amsterdam).
Faure, G., 1977. Principles of Isotope Geology. John Wiley & Sons, Inc., Singapore . 589 pp.
Faure, G., Powell, J.L., 1972. Strontium isotope geology. Minerals, Rocks and Inorganic Materials, IV. Springer Verlag, Berlin . 188 pp.
Ferreiro-Mählmann, R., 1994. Zur Bestimmung von Diagenesehöhe und beginnender Metamorphose — Temperaturgeschichte und Tektonogenese des Austroalpins und Südpenninikums in Voralberg und Mittelbünden. Frankfurter geowissenschaftliche Arbeiten, Serie C, Mineralogie 10 (Frankfurt am Main. 259 pp.).
Frank, W., Kralik, M., Scharbert, S., Thöni, M., 1987. Geochronical data from the eastern Alps. In: H.W.F, Flügel, P. (Eds.), Geodynamics of the Eastern Alps, Wien. 272–281 pp.
Frisia, S., 1994. Mechanisms of complete dolomitization in a carbonate shelf: comparison between the Norian Dolomia Principale (Italy) and the Holocene of Abu Dhabi Sabkha. In: Purser, B., Tucker, M., Zenger, D. (Eds.), Dolomites — A Volume in Honour of Dolomieu, 21. Special Publication of the International Association of Sedimentologists, Oxford, p. 451.
Frisia, S., Wenk, H.-R., 1993. TEM and AEM study of pervasive, multi-step dolomitization of the upper Triassic Dolomia Principale (Northern Italy). Journal of Sedimentary Petrology 63 (6), 1049–1058.
Fruth, I., Scherreiks, R., 1984. Hauptdolomit — sedimentary and paleogeographic models (Norian, Northern Calcareous Alps). Geologische Rundschau 73 (1), 305–319.
Füchtbauer, H., Goldschmidt, H., 1965. Beziehungen zwischen Calcium-Gehalt und Bildungsbedingungen der Dolomite. Geologische Rundschau 55, 29–40 (Stuttgart).
Füchtbauer, H., Richter, D.K., 1988. Karbonatgesteine. In: Füchtbauer (Ed.), Sedimente und Sedimentgesteine, pp. 233–434. Stuttgart.
Gaines, A.M., 1980. Dolomitization kinetics: recent experimental studies. In: Zenger, D.H., Dunham, J.B., Ethington, R.L. (Eds.), Concepts and Models of Dolomitization: Society for Sedimentary Geology. Special Publications, pp. 81–86.
Galy, A., Belshaw, N.S., Halicz, L., O'Nions, R.K., 2001. High-precision measurements of magnesium isotopes by multiple-collector inductively coupled plasma mass spectrometry. International Journal of Mass Spectrometry 208, 89–98.
Galy, A., Bar-Matthews, M., Halicz, L., O'Nions, R.K., 2002. Mg isotopic composition of carbonate: insight from speleothem formation. Earth and Planetary Science Letters 201, 105–115.
Galy, A., Yoffe, O., Janney, P.E., Williams, R.W., Cloquet, C., Alard, O., Halicz, L., Wadwha, M., Hutcheon, I.D., Ramon, E., Carignan, J., 2003. Magnesium isotopes heterogeneity of the isotopic standard SRM980 and new reference materials for magnesium-isotope-ratio measurements. Jounal of Analytical Atomic Spectrometry 18, 1352–1356.
Gawlick, H.-J., 1996. Möglichkeiten zur Abschätzung des Wärmeflusses in Sedimentbecken mit Hilfe der CAI-Methode. In: C.S., Spötl, D. (Eds.), 1. Österr. Sedimentologen-Workshop — Programm und Kurzfassungen, Seewalchen.
Gawlick, H.J., Frisch, W., 2003. The Middle to Late Jurassic carbonate clastic radiolaritic flysch sediments in the Northern Calcareous Alps: sedimentology, basin evolution, and tectonic — an overview. Neues Jahrbuch für Geologie und Paläontologie — Abhandlungen 230, 163–213 (Stuttgart).
Gawlick, H.-J., Königshof, P., 1993. Diagenese, niedrig- und mittelgradige Metamorphose in den südlichen Salzburger Kalkalpen — Paläotemperaturabschätzung auf der Grundlage von Conodont-Color-Alteration-Index-(CAI-)Daten. Jahrbuch der geologischen Bundesanstalt 136 (1), 39–48.
Gawlick, H.-J., Krystyn, L., Lein, R., 1994. Conodont Color Alteration Indices: palaeotemperatures and metamorphism in the Northern Calcareous Alps — a general view. Geologische Rundschau 83, 660–664.
Geyssant, J., 1973. Stratigraphische und tektonische Studien in der Kalkkögelgruppe bei Innsbruck in Tirol. Verhandlungen der geologischen Bundesanstalt 3, 377–396 (Wien).
Gillhaus, A., Habermann, D., Meijer, J., Richter, D.K., 2000. Cathodoluminescence spectroscopy and micro-PIXE: combined high resolution Mn-analyses in dolomites — first results. Nuclear Instruments and Methods in Physics Research B 161–163, 842–845.
Gillhaus, A., Richter, D.K., Meijer, J., 2001. Quantitative high resolution cathodoluminescence spectroscopy of diagenetic and hydrothermal dolomites. Sedimentary Geology 140, 191–199.
Graf, D.L., Goldsmith, J.R., 1956. Some hydrothermal syntheses of dolomite and protodolomite. Journal of Geology 64, 173–186.
Gregg, J.M., Sibley, D.F., 1984. Epigenetic dolomitization and the origin of xenotopic dolomite texture. Journal of Sedimentary Research 54, 907–931.
Gwinner, M.P., 1978. Geographie der Alpen: Stratigraphie, Paläogeographie, Tektonik, E. Schweizerbart'sche Verlag, Stuttgart . 480 pp.
Habermann, D., Neuser, R.D., Richter, D.K., 1996. Hochauflösende Spektralanalyse der Kathodolumineszenz (KL) von Dolomit und Calcit: Beispiele der Mn- und SEE-aktivierten KL in Karbonatsedimenten. Zentralblatt für Geologie und Paläontologie, Teil 1 145–157.
Haidinger, W., 1845. Über die Pseudomorphosen und ihre anogene und katogene Bildung. Abhandlungen der k. böhm. Gesellschaft der Wissenschaften 5 (3), 231–259.
Handy, M.R., Oberhänsli, R., 2004. Explanatory notes to the map: metamorphic structure of the Alps, age map of the metamorphic structure of the Alps — tectonic interpretation and outstanding problems. Mitteilungen der Österreichischen Mineralogischen Gesellschaft 149, 201–225.
Hardy, R., Tucker, M., 1988. X-ray powder diffraction of sediments. In: Tucker, M.E. (Ed.), Techniques in Sedimentology. Blackwell Scientific Publications, Oxford, pp. 191–228.
Henrichs, C., Richter, D.K., 1993. Hochdiagenesemuster für Triasabfolgen der Regionen Rätikon, Mittelbünden und Engadiner Dolomiten (westliche Ostalpen). Zentralblatt für Geologie und Paläontologie, Teil I (6), 689–703 (Stuttgart).
Higgins, J.A., Schrag, D.P., 2010. Constraining magnesium cycling in marine sediments using magnesium isotopes. Geochimica et Cosmochimica Acta 74, 5039–5053.
Hippler, D., Buhl, D., Witbaard, R., Richter, D.K., Immenhauser, A., 2009. Towards a better understanding of magnesium-isotope ratios from marine skeletal carbonates. Geochimica et Cosmochimica Acta 73, 6134–6146.
Iannace, A., Frisia, S., 1994. Changing dolomitization styles from Norian to Rhaetian in the southern Tethys realm. In: Purser, B., Tucker, M., Zenger, D. (Eds.), Dolomites: A Volume in Honour of Dolomieu: Special Publications. The International Association of Sedimentologists, 21, pp. 75–89.
Immenhauser, A., Holmden, C., Patterson, W.P., 2008. Interpreting the carbon-isotope record of ancient shallow epeiric seas: lessons from the Recent. In: Pratt, B.R., Holmden, C. (Eds.), Dynamics of Epeiric Seas: Geological Association of Canada Special Publication, pp. 135–174.
Immenhauser, A., Buhl, D., Richter, D., Niedermayr, A., Riechelmann, D., Dietzel, M., Schulte, U., 2010. Magnesium-isotope fractionation during low-Mg calcite precipitation in a limestone cave — field study and experiments. Geochimica et Cosmochimica Acta 74, 4346–4364.
Jacobson, A.D., Zhang, Z., Lundstrom, C., Huang, F., 2010. Behavior of Mg isotopes during dedolomitization in the Madison Aquifer, South Dakota. Earth and Planetary Science Letters 297, 446–452.
Kaczmarek, S.E., Sibley, D.F., 2011. On the evolution of dolomite stoichiometry and cation order during high-temperature synthesis experiments: an alternative model for the geochemical evolution of natural dolomites. Sedimentary Geology 240, 30–40.
Katz, A., Metthews, A., 1977. The dolomitization of $CaCO_3$: an experimental study at 252–295 °C. Geochimica et Cosmochimica Acta 41, 297–308.
Koepnick, R.B., Denison, R.E., Burke, W.H., Hetherington, E.A., Dahl, D.A., 1990. Construction of the Triassic and Jurassic portion of the Phanerozoic curve of seawater $^{87}Sr/^{86}Sr$. Chemical Geology 80, 327–349.
Korte, C., 1999. $^{87}Sr/^{86}Sr$-, $\delta^{18}O$ und $\delta^{13}C$-Evolution des triassischen Meerwassers: Geochemische und stratigraphische Untersuchungen an Conodonten und Brachiopoden. Bochumer geologische und geotechnische Arbeiten 52, 171 S (Bochum).
Korte, C.H., Kozur, H.W., Bruckschen, P., Veizer, J., 2003. Strontium isotope evolution of Late Permian and Triassic seawater. Geochimica et Cosmochimica Acta 67, 47–62 (New York).
Kralik, M., Krumm, H., Schramm, J.M., 1987. Low grade and very low grade metamorphism in the Northern Calcareous Alps and in the Greywacke Zone: illite — crystalinity data and isotopic ages. In: Flügel, H., Faupl, P. (Eds.), Geodynamics of the Eastern Alps, pp. 164–178.

Kranz, J.R., 1976. Strontium — ein Fazies-Diagenese-Indikator im Oberen Wettersteinkalk (Mittel-Trias) der Ostalpen. Geologische Rundschau 65 (1), 593–615.
Kübler, H., Müller, W.E., 1962. Die Geologie des Brenner — Mesozoikums zwischen Stubai und Pflerschltal (Tirol). Jahrbuch der Geologischen Bundesanstalt 105, 173–242 (Wien).
Kürmann, H., 1993. Zur Hochdiagenese und Anchimetamorphose in Permotrias — Sedimenten des Austroalpins westlich der Tauern. Bochumer geologische und geotechnische Arbeiten 41, 328 S (Bochum).
Kürmann, H., Richter, D.K., 1989. Zur Hochdiagenese in permo-triadischen Sedimenten der südwestlichen Ostalpen. Geologische und Paläontologische Mitteilungen 16, 160–162 (Innsbruck).
Land, L.S., 1980. The isotopic and trace element geochemistry of dolomite: the state of the art. In: Zenger, D.H., Dunham, J.B., Ethington, R.L. (Eds.), Concepts and Models of Dolomitization: Society of Sedimentary Geology. Special Publications, pp. 87–110.
Land, L.S., 1985. The origin of massive dolomite. Journal of Geological Education 33, 112–125.
Land, L.S., Hoops, G.K., 1973. Sodium in carbonate sediments and rocks: a possible index to the salinity of diagenetic solutions. Jounal of Sedimentary Petrology 43 (3), 614–617.
Li, W., Chakraborty, S., Beard, B.L., Romanek, C.S., Johnson, C.M., 2012. Magnesium isotope fractionation during precipitation of inorganic calcite under laboratory conditions. Earth and Planetary Science Letters 333–334, 304–316.
Ling, M.-X., Sedaghatpour, F., Teng, F.-Z., Hays, P.D., Strauss, J., Sun, W., 2011. Homogeneous magnesium isotopic composition of seawater: an excellent geostandard for Mg isotope analysis. Rapid Communications in Mass Spectrometry 25, 2828–2836.
Lohman, K.C., 1988. Geochemical patterns of meteoric diagenetic systems and their application to studies of paleokarst. In: James, N.P., Choquette, P.W. (Eds.), Paleokarst. Springer, Berlin, pp. 58–80.
Lokier, S., Steuber, T., 2009. Large-scale intertidal polygonal features of the Abu Dhabi coastline. Sedimentology 56, 609–621.
Lumsden, D.N., 1979. Discrepancy between thin section and X-ray estimates of dolomite in limestone. Jounal of Sedimentary Petrology 49, 429–436.
Machel, H.G., 1987. Saddle dolomite as a by-product of chemical compaction and thermochemical sulfate reduction. Geology 15, 936–940.
Magdans, U., 2005. Mechanismen der Biomineralisation von Calcit am Beispiel von Seeigel-Stacheln: Untersuchung der Wechselwirkung zwischen Sorbat-Molekülen und Calcit-Wachstumsgrenzflächen mit Oberflächen-Rötgenbeugung und numerischen Simulationen. Dissertation. Ruhr-Universität Bochum, Bochum, 220 pp.
Malone, M.J., Baker, P.A., 1999. Temperature dependence of the strontium distribution coefficient in calcite: an experimental study from 40° to 200 °C and application to natural diagenetic calcites. Journal of Sedimentary Research 69 (1), 216–223.
Malone, M.J., Baker, P.A., Burns, S.J., 1996. Recrystallization of dolomite: an experimental study from 50–200 °C. Geochimica et Cosmochimica Acta 60 (12), 2189–2207.
Matthews, A., Katz, A., 1977. Oxygen isotope fractionation during the dolomitization of calcium carbonate. Geochimica et Cosmochimica Acta 41, 1431–1438.
Mazullo, S.J., Reid, A.M., Gregg, J.M., 1987. Dolomitization of Holocene Mg-calcite supratidal deposits. Geological Society of America Bulletin 28, 224–231.
McKenzie, J.A., 1981. Holocene dolomitization of calcium carbonate sediments from the coastal sabkhas of Abu Dhabi, U.A.E.: a stable isotope study. Journal of Geology 89, 185–198.
McKenzie, J.A., 1990. Dolomites: reconciling modern sample with the ancient record. Geochemistry of the Earth's Surface and of Mineral Formation, 2nd International Symposium, Aix en Provence, France.
McKenzie, J.A., Hsü, K.J., Schneider, J.F., 1980. Movement of subsurface waters under the Sabkha, Abu Dhabi, UAE, and its relation to evaporative dolomite genesis. In: Zenger, D.H., Dunham, J.B., Ethington, R.L. (Eds.), Concepts and Models of Dolomitization, pp. 11–30.
Morrow, D.W., 1982. Diagenesis 2. Dolomite: part 2. Dolomitization models and ancient dolostones. Geoscience Canada 9 (2), 95–107.
Morse, J.W., Bender, M.L., 1990. Partition coefficients in calcite: examination of factors influencing the validity of experimental results and their application to natural systems. Chemical Geology 82, 265–277.
Müller-Jungbluth, W.-U., 1970. Sedimentologische Untersuchungen des Hauptdolomits der östlichen Lechtaler Alpen. Festband des Geologischen Instituts, 300-Jahr-Feier Univ. Innsbruck, Tirol, pp. 255–308.
Nadson, G.A., 1928. Beitrag zur Kenntnis der bakteriogenen Kalkablagerungen. Archiv für Hydrobiologie 19, 154–164.
Nernst, W., 1981. Verteilung eines Stoffes zwischen zwei Lösungsmitteln und zwischen Lösungsmittel und Dampfraum. Zeitschift für Physikalische Chemie 8, 110–139.
Neuser, R.D., Bruhn, F., Götze, J., Habermann, D., Richter, D.K., 1996. Kathodolumineszenz: Methodik und Anwendung. Zentralblatt für Geologie und Paläontologie 1, 287–306.
Nordeng, S.H., Sibley, D.F., 1993. Dolomite stoichiometry and Ostwald's step rule. Geochimica et Cosmochimica Acta 58, 191–196.
Northrop, D.A., Clayton, R.N., 1966. Oxygen isotope fractionations in systems containing dolomite. Journal of Geology 74, 174–196.
Oberhänsli, R., Bousquet, R., Engi, M., Goffé, B., Gosso, G., Handy, M., Koller, F., Lardeaux, J.-M., Polino, R., Rossi, P., Schuster, R., Schwartz, S., Spalla, I., 2004. Map of the Metamorphic Structures of the Alps. Commission de la Carte Géologique du Monde.
Pisciotto, K.A., Mahoney, J.J., 1981. Isotopic survey of diagenetic carbonates. In: Yeats, R., Haq, B. (Eds.), Initial Reports of the Deep Sea Drilling Project. US Government Printing Office, Washington, DC.
Pokrovsky, B.G., Mavromatis, V., Pokrovsky, O.S., 2011. Co-variation of Mg and C isotopes in late Precambrian carbonates of the Siberian Platform: a new tool for tracing the change in weathering regime? Chemical Geology 290, 67–74.
Preto, N., Kustatscher, E., Wignall, P.B., 2010. Triassic climates — state of the art and perspectives. Palaeogeography, Palaeoclimatology, Palaeoecology 290, 1–10.
Purser, B.H., 1973. The Persian Gulf: Holocene carbonate sedimentation and diagenesis in a shallow epicontinental sea. Springer, Berlin.
Purser, B.H., Tucker, M.E., Zenger, D.H., 1994. Problems, progress and future research concerning dolomites and dolomitization. In: Purser, B.H., Tucker, M.E., Zenger, D.H. (Eds.), Dolomites: A Volume in Honour of Dolomieu. Blackwell Scientific Publications, Oxford, pp. 3–28.
Radke, B.M., Mathis, R.L., 1980. On the formation and occurrence of saddle dolomite. Journal of Sedimentary Petrology 50 (4), 1149–1168.
Richter, D.K., 1984. Zur Zusammensetzung und Diagenese natürlicher Mg-Calcite. Bochumer Geologische und Geotechnische Arbeiten 15, 310 (Bochum).
Richter, D.K., Götte, T., Götze, J., Neuser, R.D., 2003. Progress in application of cathodoluminescence (CL) in sedimentary petrology. Mineralogy and Petrology 79, 127–166.
Riechelmann, S., Buhl, D., Schröder-Ritzrau, A., Spötl, C., Riechelmann, D.F.C., Richter, D., Kluge, T., Marx, T., Immenhauser, A., 2012. Hydrogeochemistry and fractionation pathways of Mg isotopes in a continental weathering system: lessons from field experiments. Chemical Geology 300–3001, 109–122.
Rustad, J.R., Casey, W.H., Yin, Q.-Z., Bylaska, E.J., Felmy, A.R., Bogatko, S.A., Jackson, V.E., Dixon, D.A., 2010. Isotopic fractionation of Mg^{2+} (aq), Ca^{2+} (aq), and Fe^{2+} (aq) with carbonate minerals. Geochimica et Cosmochimica Acta 74, 6301–6323.
Samtani, M., Dollimore, D., Alexander, K.S., 2002. Comparison of dolomite decomposition kinetics with related carbonates and the effect of procedural variables on its kinetic parameters. Thermochimica Acta 392–393, 135–145.
Sánchez-Román, M., Vasconcelos, C., Schmid, T., Dittrich, M., McKenzie, J.A., Zenobi, R., Rivadeneyra, M.A., 2008. Aerobic microbial dolomite at the nanometer scale: implications for the geologic record. Geology 36 (11), 879–882.
Sánchez-Román, M., McKenzie, J.A., De Luca Rebello Wagener, A., Rivadeneyra, M.A., Vasconcelos, C., 2009. Presence of sulfate does not inhibit low-temperature dolomite precipitation. Earth and Planetary Science Letters 285, 131–139.
Sánchez-Román, M., McKenzie, J.A., de Luca Rebello Wagner, A., Romanek, C.S., Sánchez-Navas, A., Vasconcelos, C., 2011. Experimentally determined biomediated Sr partition coefficient for dolomite: significance and implication for natural dolomite. Geochimica et Cosmochimica Acta 75, 887–904.
Saulnier, S., Rollion-Bard, C., Nathalie, V., Chaussidon, M., 2012. Mg isotope fractionation during calcite precipitation: an experimental study. Geochimica et Cosmochimica Acta 91, 75–91.
Schauble, E.A., 2011. First-principles estimates of equilibrium magnesium isotope fractiontation in silicate, oxide, carbonate and hexaaquamagnesium (2+) crystals. Geochimica et Cosmochimica Acta 75, 844–869.
Schmid, S., Haas, R., 1989. Transition from near-surface thrusting to intrabasement decollement, Schlinig thrust, Eastern Alps. Tectonics 8 (4), 697–718 (Washington).
Schuster, R., Koller, F., Hoeck, V., Hoinkes, G., Bousquet, R., 2004. Explanatory notes to the map: metamorphic structure of the Alps — metamorphic evolution of the Eastern Alps. Mitteilungen der Österreichischen Mineralogischen Gesellschaft 149, 175–199.
Scotese, 2000. Late Triassic Climate. http://www.scotese.com/climate.htm (accessed June 2012).
Shukla, V., 1986. Epigenetic dolomitization and the origin of xenotopic dolomite texture — discussion. Journal of Sedimentary Petrology 56 (5), 733–736.
Sibley, D.F., Gregg, J.M., 1987. Classification of dolomite rock textures. Journal of Sedimentary Research 57, 967–975.
Swart, P.K., Dawans, J.M., 1984. Variations in Mg/Ca as a control on distribution of strontium concentrations and $\delta^{18}O$ in upper Tertiary dolomites from Bahamas. American Association of Petroleum Geologists 68 (4), 533.
Taylor, J.R., 1997. An Introduction to Error Analysis — The Study of Uncertainties in Physical Measurements, 2nd edition. University Science Books, Sausalito, Canada, p. 327.
Tipper, E.T., Galy, A., Gaillardet, J., Bickle, M.J., Elderfield, H., Carder, E.A., 2006. The magnesium isotope budget of the modern ocean: constraints from riverine magnesium isotope ratios. Earth and Planetary Science Letters 250, 241–253.
Tipper, E.T., Galy, A., Bickle, M.J., 2008a. Calcium and magnesium isotope systematics in rivers draining the Himalaya–Tibetan-Plateau region: lithological or fractionation control? Geochimica et Cosmochimica Acta 72, 1057–1075.
Tipper, E.T., Louvat, P., Capmas, F., Galy, A., Gaillardet, J., 2008b. Accuracy of stable Mg and Ca isotope data obtained by MC-ICP-MS using the standard addition method. Chemical Geology 257, 65–75.
Tollmann, A., 1977. Geologie von Österreich. Deuticke, Wien.
Vahrenkamp, V.C., Swart, P.K., 1990. New distribution coefficient for the incorporation of strontium into dolomite and its implications for the formation of ancient dolomites. Geology 18, 387–391 (Boulder).
Vasconcelos, C., McKenzie, J.A., Bernasconi, S., Grujic, D., Tien, A.J., 1995. Microbial mediation as a possible mechanism for natural dolomite formation at low temperatures. Nature 377, 220–222.
Veizer, J., Ala, D., Azmy, K., Bruckschen, P., Buhl, D., Bruhn, F., Carden, G.A.F., Diener, A., Ebneth, S., Godderis, Y., Jasper, T., Korte, C., Pawellek, S., Podlaha, O.G., Strauss, H., 1999. $^{87}Sr/^{86}Sr$, $\delta^{13}C$ and $\delta^{18}O$ evolution of Phanerozoic seawater. Chemical Geology 161, 59–88.
Warren, J.K., 1991. Sulfate dominated sea-marginal and platform evaporative settings. In: Melvin, J.L. (Ed.), Evaporites, Petroleum and Mineral Resources. : Developments in Sedimentology, 50. Elsevier, Amsterdam.
Warren, J., 2000. Dolomite: occurrence, evolution and economically important associations. Earth-Science Reviews 52, 1–81.
Warthmann, R., Van Lith, Y., Vasconcelos, C., McKenzie, J.A., Karpoff, A.M., 2000. Bacterially induced dolomite precipitation in anoxic culture experiments. Geology 28 (12), 1091–1094.

Wheeler, C.W., Aharon, P., Ferrell, R.E., 1999. Successions of Late Cenozoic platform dolomites distinguished by texture, geochemistry, and crystal chemistry: Niue, South Pacific. Journal of Sedimentary Research 69 (1), 239–255.
Wombacher, F., Eisenhauer, A., Heuser, A., Weyer, S., 2009. Separation of Mg, Ca and Fe from geological reference materials for stable isotope ratio analyses by MC-ICP-MS and double-spike TIMS. Journal of Analytical Atomic Spectrometry 24.
Wombacher, F., Eisenhauer, A., Böhm, F., Gussone, N., Regenberg, M., Dullo, W-Chr, Rüggeberg, A., 2011. Magnesium stable isotope fractionation in marine biogenic calcite and aragonite. Geochimica et Cosmochimica Acta 75 (19), 5797–5818.
Young, E.D., Galy, A., 2004. The isotope geochemistry and cosmochemistry of magnesium. Reviews in Mineralogy & Geochemistry 55, 197–230.
Zankl, H., 1971. Upper Triassic carbonate facies in the Northern Limestone Alps. In: Müller, G. (Ed.), Sedimentology of Parts of Central Europe. Guidebook. VIII. International Sedimentary Congress, pp. 147–185.
Zattin, M., Cuman, A., Fantoni, R., Martin, S., Scotti, P., Stefani, C., 2006. From Middle Jurassic heating to Neogene cooling: the thermochronological evolution of the southern Alps. Tectonophysics 414, 191–202.
Zeebe, R.E., 2001. Seawater pH and isotopic paleotemperatures of Cretaceous oceans. Palaeogeography, Palaeoclimatology, Palaeoecology 170 (1–2), 49–57.
Zeeh, S., 1998. Karbonatzemente als Indikatoren des Fluid-Flow während der alpinen Orogenese in den Ost- und Südalpen. Gaea heidelbergensis 5, 168 (Heidelberg).
Zeeh, S., 2000. Timing of cement precipitation and fault activity in the Eastern and Southern Alps (Austria, Germany, Italy and Slovenia). Journal of Geochemical Exploration 69–70, 585–588 (Amsterdam–New York).
Ziegler, P.A., 1988. Evolution of the Arctic-North Atlantic and the Western Tethys. American Association of Petroleum Geologists 43 (198 pp. Tulsa).
Zorlu, J., 2006. Sedimentpetrographische und geochemische Untersuchungen an unterschiedlich überprägten Triasdolomiten der Ost- und Südalpen. Dissertation. Ruhr-Universität Bochum, Bochum, pp. 163.
Zorlu, J., Götte, T., Richter, D.K., 2007. Diagenesemuster in oberladinischen Sabkhadolomiten des Jaggl am Reschensee (W'Zentralalpen). Journal of Alpine Geology 48, 7–22.